Chapter 6
Nanomaterials for X-Ray Nanochemistry

It takes strength to speak one's mind. It takes skill to communicate.

6.1 Introduction

The nanomaterials used in the initial experiments of X-ray nanochemistry were small gold nanoparticles. Guo stated in his 2001 proposal that less than 3 nm gold nanoparticles were ideal because the originally perceived enhancement was derived only from electrons released from nanoparticles upon X-ray absorption by these nanoparticles. Without performing numerical simulations, it was estimated that the smaller the nanoparticles, the more electrons, including Auger and secondary electrons, could escape from the nanoparticles and deposit energy into the surrounding medium such as water or tissues. Therefore, in their first publication, Guo et al. [1] used 5 nm gold nanoparticles synthesized based on a method developed by Brust et al. [2]. Similarly, Hainfeld et al. [3] chose 1.9 nm gold nanoparticles in their first work. The company formed by Hainfeld et al. (Nanoprobe Inc.) manufactured and sold 1.9 nm gold nanoparticles to many groups, which used these 1.9 nm nanoparticles to measure enhancement.

Based on the results presented in Chaps. 2, 3, 4, and 5, it is clear that the size of gold nanoparticles affects the number and energy spectrum of electrons escaping from gold nanoparticles. Large nanoparticles (up to 100 nm dia.) may retain a significant fraction (up to 25%) of energy due to electron energy loss in these nanoparticles. Small nanoparticles, especially less than 5 nm metal nanoparticles, have negligible electron retention. However, contrary to the original expectations, these small gold nanoparticles may not exhibit meaningful physical enhancement unless at high concentrations, at which the surface area of these nanoparticles is so large that other properties, such as scavenging or catalytic functions, overwhelm physical enhancement. Further, these small nanoparticles may interact strongly with many probe molecules, such as DNA molecules, repair proteins, or coumarin-3-carboxylic acid (3-CCA) and its intermediates. The size of nanoparticles also controls cellular uptake as these small sizes may not be ideal for maximum cellular

T. Guo, *X-ray Nanochemistry*, Nanostructure Science and Technology,
https://doi.org/10.1007/978-3-319-78004-7_6

uptake as demonstrated by many reports including Chithrani et al. [4]. In a more recent publication, Hainfeld et al. [5] used 11 nm gold nanoparticles instead of 1.9 nm gold nanoparticles. On the other hand, large nanoparticles may have solubility problems, especially in applications that require long circulation times. For several reasons, such as maximum uptake by cells or minimal chemical enhancement, the ideal particle size for creating strong physical enhancement is 50 nm. On the other hand, the ideal size for chemical enhancement is less than 10 nm, possibly below 5 nm. These results demonstrate the importance of selecting the right size of nanomaterials for applications in X-ray nanochemistry. For this reason, nanomaterials used in X-ray nanochemistry and their synthesis are reviewed here based on their sizes.

In addition to the particle size that can affect the percentage and energy spectrum of escaping electrons, other parameters such as surface area, surfactants, composition, and shape of the nanomaterials can also affect the magnitude of enhancement, especially chemical and possibly biological enhancement. For type 3 physical enhancement, there is no ideal size, at least not yet being claimed, although crystallinity can be an important factor. These properties as well as how surfactants are chemically attached to the surface of nanoparticles are briefly reviewed in this chapter.

Many types of nanomaterials have been used to generate the enhancement in the context of X-ray nanochemistry, and this chapter summarizes these nanomaterials, which are a very small subset of the nanomaterials that have been synthesized since the beginning of the era of nanotechnology and nanoscience. Several books and reviews, such as those by Ozin and Arsenault [6] and El-Sayed et al. [7], are available, which discuss synthesis, properties, and applications of these nanomaterials. In this chapter, the emphasis is placed on discussion of the nanomaterials that have been used in measuring enhancements defined in X-ray nanochemistry. Alternative nanomaterials are mentioned whenever appropriate.

Methods used for characterization of these nanomaterials are briefly mentioned as well. The characterization parameters are similarly chosen to reflect their prominence in controlling the enhancement. However, such a choice is based on current published results, therefore having its limitations and may change in the future. Special characterization methods may be invented in the future for the purpose of uncovering the origins of enhancement.

6.2 Nanomaterial Properties

It is desirable to use a set of parameters to define the structure of a nanomaterial. Once these parameters are found, they can be conveniently used to infer the properties of the nanomaterial because the structure of a nanomaterial usually determines its properties. From X-ray nanochemistry perspective, these parameters, either in part or whole, can influence the enhancement by the nanomaterial. In addition to defining nanomaterials, these parameters may also be used to refine the control of interactions between nanomaterials and their surroundings, such as

Table 6.1 Parameters used to define the nanomaterials that have been used in the enhancement measurement in X-ray nanochemistry

Parameters	Range	Properties
Radius	0.1–1000 nm	Surface-to-volume atoms, surface area, X-ray absorption, cellular uptake, solubility, surface plasmon response
Shape	Aspect ratio (rods), thickness/length (prisms)	Surface plasmon response
Composition	Elemental, oxide, polymer	Mobility in solution
Surface	Metal and oxide	Catalytic
Surfactants	Metal, functional groups, and oxide	Solubility, mobility, scavenging
Alloy	2–4 elements	Catalytic, surface plasmon response
Core-shell	Number and thicknesses	Protection of surface (oxide), surface plasmon response
Aggregates	2–1000	Nanoparticles mass, surface plasmon response, other nanostructures

proteins, DNA, other molecules, or nanomaterials. However, not all the parameters are yet known to researchers. For example, the structural parameters critical to influencing chemical enhancement are only speculated but not well defined. Another example of difficult-to-define parameters is that some properties are a continuous function of the structural parameters, thereby creating a situation where nearly an infinite number of parameters are needed to define a nanomaterial. In these cases, currently available parameters may be insufficient to define the nanomaterial, or the parameters are insufficiently defined.

Seven generic parameters used to define a nanomaterial are given in Table 6.1, which include the radius/dimension, shape (including aspect ratio, thickness, etc., depending on the shape and structures), composition, surface coverage of surfactants, alloy, core-shell, and aggregates. Table 6.1 also lists the connections between the properties and parameters, although the properties shown in the list are not exhaustive. There may be other parameters derived from the ones listed in the table that can be used to better define the nanomaterials. Among the parameters listed in Table 6.1, surface-to-volume ratio and total surface area per unit mass are commonly used in X-ray nanochemistry. Though useful, other parameters are difficult to define. For example, crystallinity is one such parameter that can affect the type 3 physical enhancement or magnetic response of nanomaterials. Other parameters, such as the profile of UV-Vis or SERS spectra, may also be important but are not listed in Table 6.1. Another parameter or even a set of parameters is that defines the carrier(s) of nanomaterials, whether it is pure water or aqueous solutions. Unfortunately, this parameter is usually not specified clearly enough to enable researchers to consider its impact on enhancement. In the future, a set of parameters may be attached or associated to each nanomaterial so that a specific nanomaterial can be readily defined based on these parameters in a necessary and sufficient way.

In the following, four major categories of nanomaterials and their syntheses are briefly discussed.

6.3 Nanomaterials and Syntheses

Four major categories of nanomaterials discussed in this section have been used in enhancement measurements reported in the literature. They are (1) spherical nanoparticles, (2) nonspherical nanoparticles, (3) aggregates of the same nanoparticles, and (4) assembly of different nanomaterials. The majority of nanomaterials are spherical, including alloy and core-shell- and liposome- or micelle-based nanomaterials.

6.3.1 Spherical Nanoparticles

The most popular nanomaterials are spherical nanoparticles, which include quantum dots, metal and semiconductor nanoparticles, core-shell structures, liposomes and micelles, and polymer-based nanoparticles. Nanomaterials discussed here have been used in enhancement measurements in the context of X-ray nanochemistry. The intended enhancements include types 1, 2, and 3 physical enhancement and types 1 and 2 chemical enhancement. To date, there are only several intended uses of these nanoparticles for biological enhancement as discussed in Chap. 4 (e.g., see Figs. 4.4 and 4.5). The spherical nanoparticles are reviewed according to their composition.

6.3.1.1 Gold Nanoparticles

The discussion here is arranged according to the size of gold nanoparticles, from the smallest to the largest. The nanoparticles developed or used by a particular group are discussed in tandem. This is similar to the style used throughout this book.

Gold nanoparticles are the most popular spherical nanoparticles used in X-ray nanochemistry as reported in the literature. Several reviews are available. Brust el al. [8] summarized the literature on the synthesis and self-assembly of these nanoparticles. A review of applications of gold nanoparticles was given by Forbes et al. [9]. Another review was written by El-Sayed and Murphy et al. [7], which covered almost all gold nanoscale species. The methods of synthesis were generally not invented by the researchers working in the field of X-ray nanochemistry. There were a few exceptions, however, in which nanomaterials were either made for the first time for the use in X-ray nanochemistry or were refined to become more suitable for enhancement measurements. In addition, nanoparticles made according to the methods reported in the literature often require further modifications to suit for applications in X-ray nanochemistry. However, there

are no full-scale reviews on gold nanoparticle synthesis for X-ray nanochemistry. Here, a brief summary of gold nanoparticle synthesis is given specifically for measuring X-ray nanochemical enhancement.

There are many sizes and coatings of spherical gold nanoparticles, ranging from a few scores of atoms to 1.9 nm in diameter, to more than 300 nm in diameter. The smallest gold nanoparticles only had 29–43 gold atoms. They were synthesized by Xie et al. [10] using a method of adding chloroauric acid into glutathione (GSH) aqueous solutions at 25 °C followed by reaction at 70 °C for 24 h. $Au_{29–43}$ nanoclusters coated with GS ligands were obtained.

Other small gold nanoparticles have been made. Small gold nanoparticles were synthesized by Nanoprobes, Inc. The most recent name for this nanoparticle is AuroVist™ and is marketed mainly as a contrast agent for transmission electron microscopy and microCT. These small nanoparticles were highly soluble (>15 WP) in blood as well as in water, which made them suitable for imaging. For X-ray nanochemistry, these small nanoparticles may be more prone to cause chemical and biological enhancement than physical enhancement as discussed in Chaps. 2, 3, 4, and 5. The synthetic procedure was not reported, but Brust et al. [2] reported synthesis of 1–3 nm gold nanoparticles. The synthesis reported by Brust et al. was performed in a two-phase, organic and aqueous, solvent system. The results are shown in Fig. 6.1.

Hainfeld et al. [5] used 11 nm gold nanoparticles for enhancement of radiotherapy to treat brain tumors in mice. Nanomaterial synthesis was not disclosed, but as shown before and here in this section, gold nanoparticles whose size ranged from 3 to 300 nm were made and used in various enhancement measurements. Even though the nanoparticles used in many studies were purchased, to date there is no direct evidence to suggest that these purchased gold nanoparticles are substantially different from those synthesized using the disclosed methods.

In a series of publications, Guo et al. synthesized gold nanoparticles ranging from 3 to 150 nm in diameter and used them in studies of X-ray nanochemistry. Guo et al. [1] developed a method that was the combination of the approaches developed by Whitesides et al. [11], Brust et al. [2], and Rotello et al. [12]. The method allowed Guo et al. [1] to make 5.6 nm trimethylammonium (TMA) dodecanethiol-covered

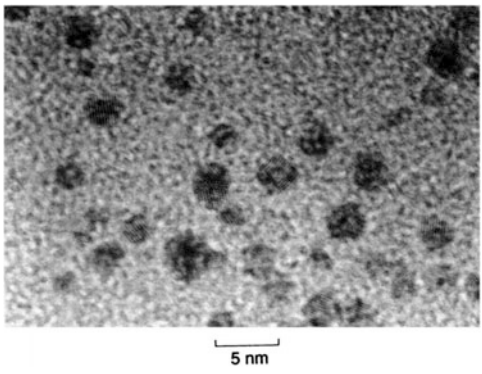

Fig. 6.1 1–3 nm gold nanoparticles synthesized by Brust et al. [2]. A TEM image of the nanoparticles is shown here. (Adapted from Brust et al. [2] with permission of the Royal Society of Chemistry.)

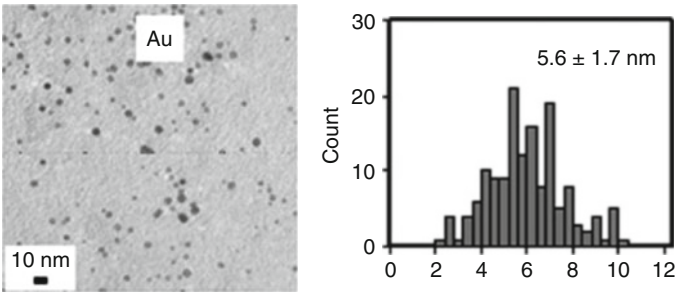

Fig. 6.2 5.6 nm gold nanoparticles synthesized by Guo et al. [1]. A TEM image is shown in the left panel and size distribution is shown in the right panel. (Adapted from Guo et al. [1] with permission of the Royal Society of Chemistry.)

gold nanoparticles. The key step of the synthesis was the attachment of thiol ligands to gold nanoparticles as the zero-valent gold nanoparticles were formed. Gold ions were reduced by sodium borohydride, and the nanoparticles were readily covered with tetraoctylammonium ligands. Once covered, the nanoparticles were transferred automatically to an organic solvent phase. These nanoparticles can be coated with other ligands using ligand exchange reactions as explained later in this section. The nanoparticles were used in enhanced DNA strand break measurements under X-ray irradiation. These nanoparticles are shown in Fig. 6.2.

Guo et al. [13] adopted methods to synthesize 3, 7, and 30 nm gold nanoparticles. The 3 nm gold nanoparticles were synthesized by adopting a method developed by Baiker et al. [14, 15] using sodium hydroxide as the reducing agent and tetrakis-hydroxymethyl-phosphonium chloride (THPC) as the protection ligand. The authors also synthesized 7 nm gold nanoparticles by first reducing gold ions with sodium citrate and then sodium borohydride. Polyethylene glycol (PEG) or mercaptopropionic acid (MPA) ligands were used to protect the surface of the gold nanoparticles. For larger gold nanoparticles, such as 30 nm gold nanoparticles, modified Turkevich method from the original Turkevich method [16] was used. In another work, 16 nm gold nanoparticles were synthesized for conjugation of DNA molecules to the surface of gold nanoparticles, and results were published by Guo et al. [17]. The nanoparticles are shown in the left panel of Fig. 6.3. Larger 88 nm gold nanoparticles were synthesized based on a seed growth method developed by Perrault and Chan [18], and the approach was used to prepare large gold nanoparticles by Guo et al. [19]. Figure 6.3 (right panel) shows the gold nanoparticles made by Chan et al. The seed growth method was particularly effective in producing uniformly sized 88 nm gold nanoparticles. The 88-nm diameter gold nanoparticles are shown in Fig. 6.10 and are covered with a silica layer.

Hwu et al. in Wang et al. [20] and Liu et al. [21] as well as in Liu et al. [22] showed the results of synthesis of PEGylated gold nanoparticles under synchrotron X-ray irradiation and then used the nanoparticles for enhancement measurements. The synthesis was similar to reduction of gold salts in aqueous solutions, except that

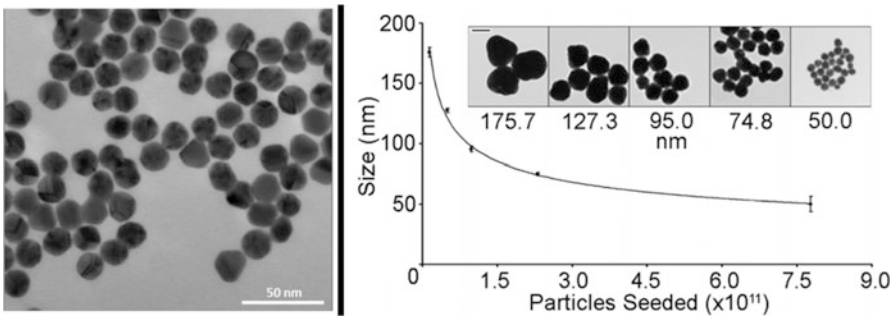

Fig. 6.3 16 nm gold nanoparticles synthesized by Guo et al. [17], and 50–200 nm gold nanoparticles by Perrault and Chan [18]. (Left panel: Adapted from Guo et al. [17] with permission of the Royal Society of Chemistry. Right panel: Adapted with permission from Perrault and Chan [18]. Copyright (2009) American Chemical Society.)

the reducing agent were the chemicals produced in water under X-ray radiation. The size of gold nanoparticles ranged from 15 to 18 nm. The gold nanoparticles were used to obtain enhancement of X-ray radiation effect on damaging cells. Kumar et al. [23] discussed what the authors called third-generation gold nanoparticles optimized for radiation therapy. The authors first obtained THPC-covered small gold nanoparticles. The second step of PEGylation was used to cover the surface of nanoparticles with PEG ligands to increase solubility. The size of these gold nanoparticles was small, between 1 and 3 nm, far below the optimal size of gold nanoparticles for maximum uptake by cells as found by Chithrani et al. [4]. Their optimization was conducted according to three parameters: (1) surfactants, (2) nanoparticle size, and (3) magnitude of enhancement.

"Naked" gold nanoparticles were made by Hwu et al. [24] and Meisel et al. [25]. The latter followed a method developed by Evanoff and Chumanov for making silver nanoparticles [26]. The method involved reaction of Au_2O_3 with H_2 for 10 min. The authors reported the formation of 20–100 nm gold nanoparticles. A size distribution is shown in Fig. 6.4.

Several groups have developed methods to synthesize large gold nanoparticles that can be used in physical enhancement measurements. For example, Eychmuller and Ziegler [27] reported the synthesis of gold nanoparticles ranging from 15 to 300 nm. The authors adopted the seed growth method in which gold nanoparticle seeds were made using the citrate reduction method. Subsequent growth to form larger gold nanoparticles was accomplished using trisodium citrate and ascorbic acid to reduce gold ions. Figure 6.5 shows several different sizes of gold nanoparticles. Any of these nanoparticles may be used for enhancement measurements, though none of them has been used. Their methods can be compared to Puntes et al. [28], who also discussed synthesis of up to 200 nm gold nanoparticles. Puntes et al. employed only sodium citrate but adopted a more elaborate gold salt addition and temperature control scheme. Another example was given by Wang et al. [29] who also demonstrated a method with which they synthesized gold nanoparticles using a

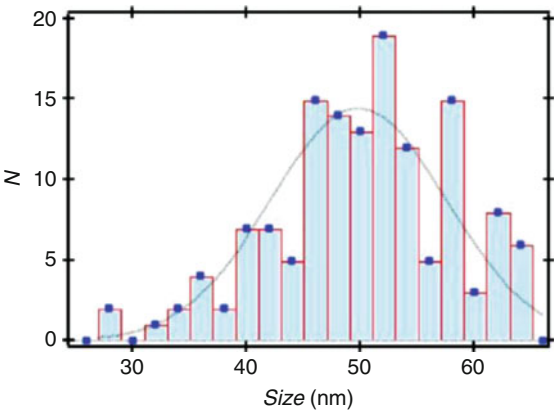

Fig. 6.4 20–100 nm "naked" gold nanoparticles synthesized by Meisel et al. [25]. (Adapted with permission from Meisel et al. [25]. Copyright (2010) American Chemical Society.)

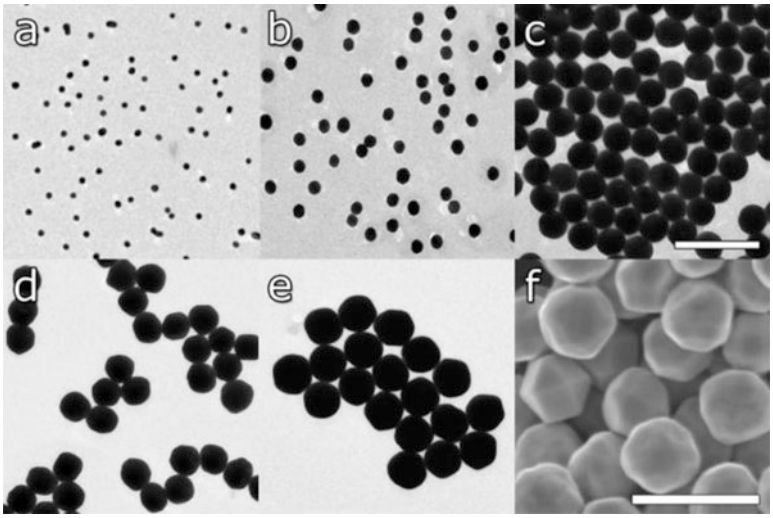

Fig. 6.5 15–300 nm gold nanoparticles synthesized by Eychmuller and Ziegler. The figure shows TEM images of 15, 31, 69, 121, and 151 nm and SEM image of 294 nm gold nanoparticles. The scale bars are 200 nm for (**a–c**) and 500 nm for (**d–f**). (Adapted with permission from Eychmuller and Ziegler [27]. Copyright (2011) American Chemical Society.)

seed growth method from 12 nm diameter citrate-covered gold nanoparticles. The final size ranged from 30 to 220 nm in diameter. The seeded growth was carried out using H_2O_2 as the reducing agent. In addition to gold salt and H_2O_2, citrate was also added. The shape was quasi-spherical.

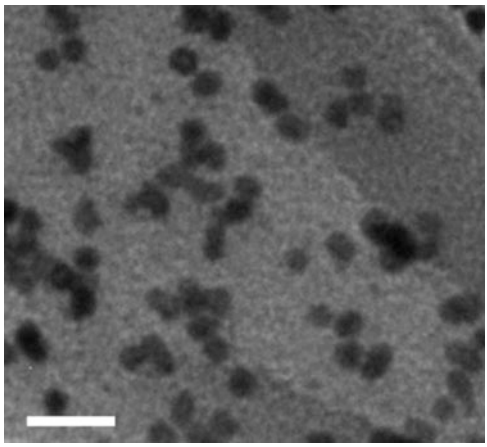

Fig. 6.6 5 nm Pt nanoparticles used in the work published by Guo et al. [13]. The scale bar is 20 nm

6.3.1.2 Platinum Nanoparticles

Platinum nanoparticles resemble gold nanoparticles in many ways. However, its popularity has not yet reached a comparable status to gold nanoparticles because platinum nanoparticles of different sizes and surface coverage are more difficult to prepare. In the enhancement measurement work presented by Guo et al. [13], the author adopted a method developed by Somorjai et al. [30]. Platinum salt was reduced by sodium hydroxide in ethylene glycol solution. Approximately 1–5 nm diameter platinum nanoparticles were made, depending on the synthetic condition. The nanoparticles were then protected by polyvinylpyrrolidone (PVP, MW 29,000) in HCl ethanol solution. Figure 6.6 shows a TEM image of the nanoparticles. The average size was 5 nm.

6.3.1.3 Silver Nanoparticles

Silver nanoparticles were used in enhancement measurements using synchrotron X-rays by Guo et al. [13]. The nanoparticles were the same as those used in surface-enhanced Raman spectroscopy (SERS) measurements performed by Guo et al. [31]. Synthetic methods were essentially the same as the methods used to synthesize gold nanoparticles, which were made from citrate reduction of gold salt in aqueous solutions, a method adopted from an approach reported by Scherer et al. [32]. These silver nanoparticles were protected by citrate ligands. Guo et al. (unpublished) also synthesized bare silver nanoparticles using sodium borohydride as the reducing agent. The synthesis was performed in silver salt solutions in an ice-water chilled bath, a method first reported by Solomon et al. [33]. These silver nanoparticles were large, 30 ± 6 nm, as shown in Fig. 6.7.

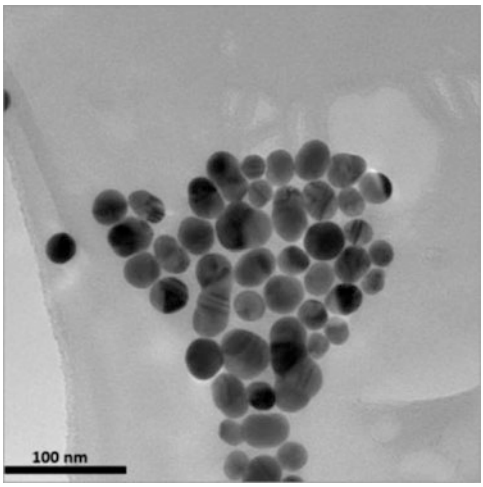

Fig. 6.7 Silver nanoparticle synthesized by Guo et al. and used in the work published by Guo et al. [13]. The average size is 30 nm and the scale bar is 100 nm

6.3.1.4 Bismuth Nanoparticles

Bismuth nanoparticles were used in enhancement measurements. For example, Li et al. [34] made 3–4 nm bismuth nanoparticles for targeted delivery and in vitro and in vivo studies. The nanoparticles were synthesized at 260 °C in oleylamine solutions, a method commonly used in transition metal nanoparticle syntheses.

6.3.1.5 Silver-Core-Gold-Shell Nanoparticles

Metallic nanoparticles commonly have residual electric charges left on them after reduction of ions. Although this is not a problem in most applications, oxidation of the aniline monomers on the surface of nanoparticles by reactive oxygen species such as hydroxyl radicals was sensitive to such residual charges, which was demonstrated by Guo et al. [35]. For this reason, a silver core was added to gold nanoparticles to take away excessive positive charges from gold because silver has a slightly lower reduction potential.

The synthesis of core-shell structure is as follows. First, silver nanoparticles (AgNPs) were made. Gold salt was then added and reduced in the presence of AgNPs to form gold nanoshells (AuNSs). It is speculated that charges on AgNP@AuNSs reside on Ag, which can be represented as $AgNP^{+}$@AuNSs. The silver-core-gold-shell nanostructures are different from gold core, silver shell nanostructures (AuNP@AgNSs), which were prepared by Shankar et al. [38]. According to the authors, charges possessed by the latter seem to reside on the gold core rather than the silver shell, which should be represented as $AuNP^{+}$ @AgNSs. It is unknown if neither, either, or both are correct, and confirmation requires direct experimental measurements in the future. Figure 6.8 shows silver-core, gold-shell spherical nanoparticles synthesized by Guo et al. [35]. These

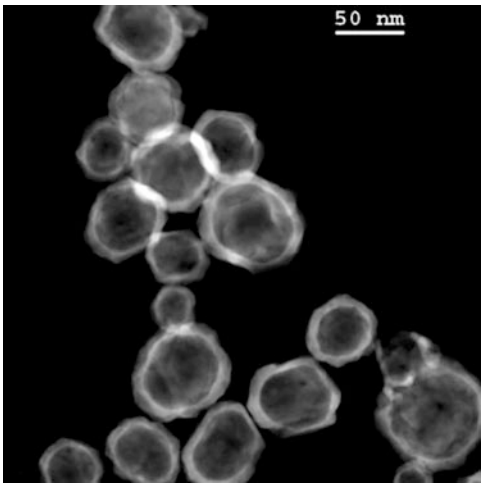

Fig. 6.8 Gold-shell-silver-core spherical nanoparticles used to demonstrate type 1 chemical enhancement of polymerization of the aniline monomers, which was detected by SERS. (Adapted with permission from Guo et al. [35]. Copyright (2012) American Chemical Society.)

nanostructures also supported strong surface-enhanced Raman spectroscopy (SERS) processes, especially when they aggregated. SERS was used to probe the product of polymerization reaction of the aniline monomer.

6.3.1.6 Liposomes and Calcium Phosphate Enclose Liposomes

Calcium phosphate-enclosed liposomes (CaPELs) have been made as nanoscale probes to detect or measure type 2 physical enhancement by Guo et al. [36]. Sulforhodamine B (SRB) aqueous solution was first entrapped in liposomes formed from phospholipids in aqueous solutions. After extrusion, uniformly sized liposomes were formed, as shown in Fig. 6.9 (panel A or left panel). Then calcium chloride and phosphoric acid were added to the solution at pH 10 to grow a layer of calcium phosphate (CaP) on the exterior of the liposomes, facilitated by the phosphate end group of the lipids. Once the desired CaP thickness was reached, 2-carboxyethylphosphonic acid (CEPA) was added. Figure 6.9 (panel B or right panel) shows the final product. CaP shell safely protects the inner aqueous solution of SRB from chemical enhancement. As a result, this nanoscale probe is ideal to study type 1 or 2 physical enhancement.

6.3.1.7 Silica-Covered Gold Nanoparticles

In order to measure type 1 physical enhancement, nanomaterials with inert surfaces are needed. However, even PEGlyated gold nanoparticles may generate type 2 physical enhancement as well as chemical enhancement. To isolate type 1 physical enhancement from other enhancements, one option is to coat an inert oxide layer

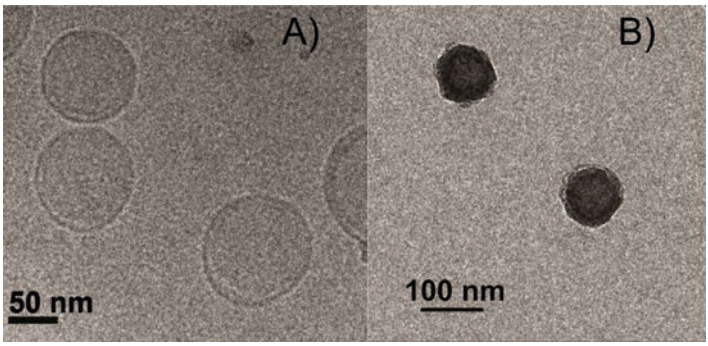

Fig. 6.9 Liposomes (A or left panel) and calcium phosphate-covered liposomes (B or right panel). The calcium phosphate-enclosed liposomes (CaPELs) were used to probe nanoscale energy deposition by nanomaterials. The results of enhancement measurements using these nanoscale probes are shown in Figs. 2.40 and 2.41. (Adapted with permission from Guo et al. [36]. Copyright (2016) American Chemical Society.)

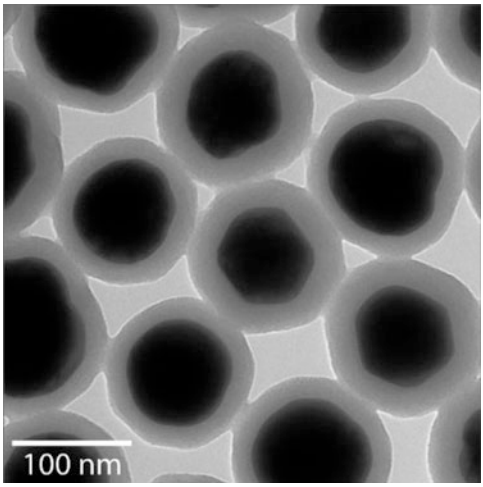

Fig. 6.10 Silica-covered gold nanoparticles by Guo et al. [19]. The gold nanoparticles were made using a seed growth method developed by Perrault and Chan [18]. Silica coating was then conducted. (Adapted with permission from Guo et al. [19]. Copyright (2014) American Chemical Society.)

onto large gold nanoparticles. Silica is a viable candidate for such coverage. Figure 6.10 shows the results of silica-covered gold nanoparticles synthesized by Guo et al. [19]. The large gold nanoparticles were made from the seed growth method mentioned earlier. Two methods of silica layer growth were used. One related to using ammonium to reduce TEOS to form relatively thick silica layers, and the other was to use arginine to reduce TEOS to form thin layers of silica as reported by Kraus et al. [37]. The latter can coat a thin layer (<4 nm) silica onto gold nanoparticles.

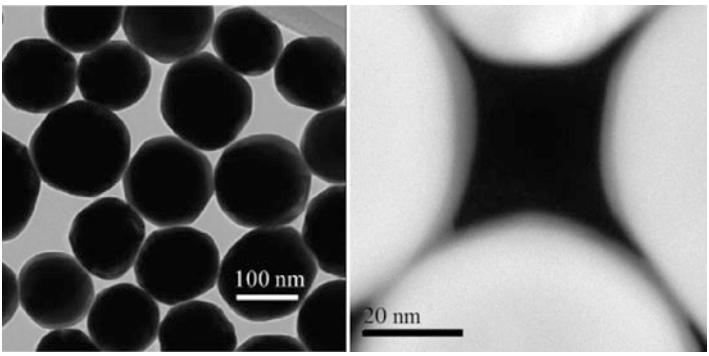

Fig. 6.11 Silver-covered gold spherical nanoparticles (Agu). The gold nanoparticles were made using a seed growth method developed by Perrault and Chan [18]. Silver coating was then conducted. (Reprinted from Guo et al. [39]. Copyright (2016) with permission from Elsevier.)

6.3.1.8 Silver-Coated Gold Nanoparticles (Agu)

Silver-coated gold nanoparticles have been synthesized by several groups. For example, as mentioned above, Shankar et al. [38] found that silver on gold nanoparticles was more resistive to chemical oxidation. Guo et al. [39] synthesized a special nanostructure called Agu that had a thin layer (<2 nm) of silver covering large (>50 nm diameter) spherical gold nanoparticles. When the thickness was between 0.5 and 2 nm for 100 nm diameter gold nanoparticles, change of surface plasmon resonance peak position followed a sigmoidal profile as a function of Ag thickness on Au. The nanomaterials were used to detect etching of silver by X-ray irradiation, as shown in Sect. 11.4. In the synthesis, gold nanoparticles were first synthesized, followed by adding Ag salt into a reducing environment of ascorbic acid. The concentration of gold nanoparticles was high so that reduced Ag ions were immediately coated onto gold nanoparticles rather than forming small silver nanoparticles en masse. Figure 6.11 shows the results. The light gray color in both left and right panels indicates the silver layer.

6.3.1.9 Palladium-Coated Hollow Gold Nanoparticles

Hao, Sun, and Mao et al. [40] synthesized hollow gold nanoparticles using reduction of gold salt in the presence of hydrogen nanobubbles. The method was first established by the authors in 2009 (see Huang et al. [41]). Hao and Sun et al. [42] used a similar method to prepare palladium-coated hollow gold nanoparticles for treating tumors. The authors first prepared the hollow gold shells. The gold shells were 25 nm thick with a 50 nm inner diameter. Then copper was coated onto the surface of hollow gold nanoparticles, followed by galvanic replacement of Cu with ^{103}Pd, which emits 21 keV X-rays with a 16-day half-life.

6.3.1.10 Oxide Nanoparticles

These are nonmetal oxide nanoparticles. For example, silica nanoparticles are available from many manufacturers. Aldrich produces SM-30, HS-40, and TM-50, which were used by Meisel et al. [43] in their radiolysis measurements. These nonmetal oxide nanoparticles were only occasionally used in enhancement measurements described in Chaps. 2, 3, 4, and 5, and most of these nanoparticles were considered inert or non-catalytic in terms of generating the enhancement as defined in X-ray nanochemistry. Therefore, the discussion is limited to the applications of radiolysis.

6.3.1.11 Transition Metal Oxide Nanoparticles

Many transition metals can potentially be used to generate the enhancement defined in this book. In a recent work, Sasaki et al. [44] utilized a unique transition metal nanomaterial, titanium peroxide (TiO_x) nanoparticles, to create enhancement to the effectiveness of X-ray irradiation. The nanoparticles were modified from anatase titanium oxide TiO_2 nanoparticles by first costing TiO_2 nanoparticles with polyacrylic acid (PAA) and then treating the nanoparticles with peroxide H_2O_2. As shown in Fig. 6.12, the nanoparticles are highly porous or gel-like. The average size measured using dynamic light scattering (DLS) was 50 nm, as shown in the right panel of Fig. 6.12. Enhancement of radiotherapy was measured using tumor cells and tumors in mice.

Chen et al. [45] synthesized mesoporous tantalum oxide nanoparticles (m-Ta_2O_5) and used them to improve the effectiveness of chemoradiotherapy. The authors coated the surface of the 60-nm diameter nanoparticles with PEG ligands (m-Ta_2O_5-PEG) followed by loading doxorubicin (DOX) into the nanoparticles (m-Ta_2O_5-PEG/DOX). The final size was close to 90 nm in diameter. The drug

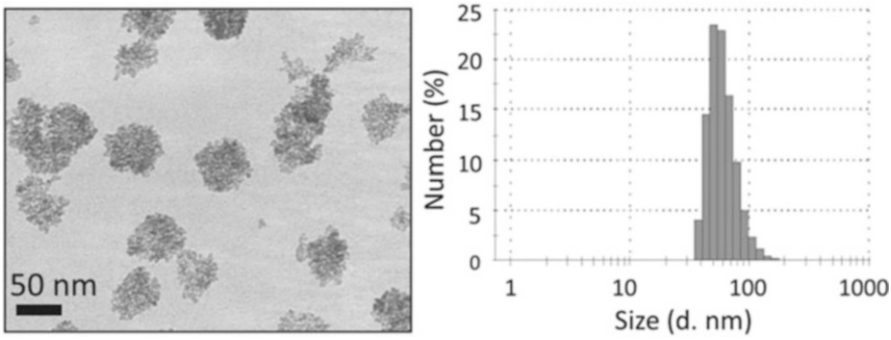

Fig. 6.12 Titanium peroxide nanoparticles produced from anatase titanium oxide (TiO_2) nanoparticles. A TEM image is shown in the left panel. The average size was 50 nm based on DLS measurements, as shown in the right panel. (Adapted with permission from Sasaki et al. [44]. Open Access under CC BY 4.0 International License.)

was completely released within 5 min when pH was lowered from 7.4 to 5.0. No toxicity was observed with the m-Ta_2O_5-PEG. Best results were obtained with m-Ta_2O_5-PEG/DOX under X-ray irradiation, which based on the data was equivalent to the addition of DOX and m-Ta_2O_5-PEG under X-ray irradiation.

6.3.1.12 Rare Earth Oxide Nanoparticles

A large number of rare earth nanoparticles have been synthesized. These nanoparticles can strongly absorb X-rays and subsequently emit UV light, which is responsible for type 3 physical enhancement described in Chap. 2. The light emission mechanisms associated with rare earth nanoparticles are associated with different quantum dots. Generally speaking, rare earth nanoparticles emit line emissions of atomic natural linewidths, whereas quantum dot emission is a narrow band of a few nanometers in bandwidth. Among these rare earth nanoparticles, several of them have been used in enhancement studies.

Cao et al. [46] discussed the preparation of Gd_2O_2S:Tb nanoparticles. Tb^{3+} ions were doped to improve luminescence. The nanoparticles were more homogeneous because of the presence of sulfur. The nanoparticles were directly used to generate type 3 physical enhancement. In another study, rare earth-doped semiconductor nanoparticles were made by Townley et al. [47]. The nanoparticles were used to augment radiotherapy in vivo. Specifically, the authors used Gd-doped TiO_2 nanoparticles as an enhancer for type 3 physical enhancement. The nanoparticles were aggregates. Synthesis was achieved by mixing various rare earth nitrate salts (hydrate) with titanium isopropoxide and isopropanol. The precipitate was then washed and treated to obtain nanoparticles, which were then covered with a silica layer or fluorescent molecules. These nanoparticles were then tested in vitro for their enhancement properties in reducing cell viability under X-ray irradiation. Yang et al. [48] developed a LaF_3:Tb@SiO_2/dye nanoparticle system to enhance X-ray-induced photodynamic therapy efficacy. Figure 6.13 shows the TEM images of nanoparticles.

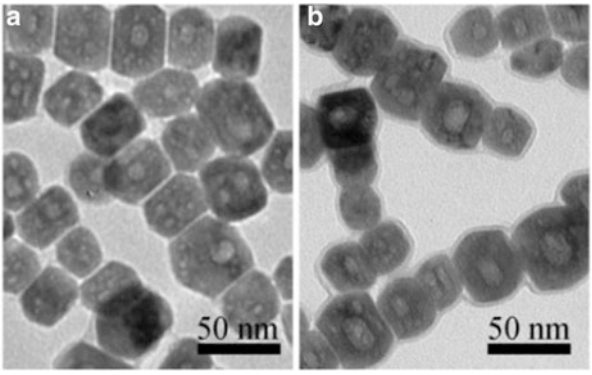

Fig. 6.13 Lanthanide-doped fluorides nanoparticles (**a**) and silica coated such nanoparticles (**b**). (Adapted from Yang et al. [48] with permission of the Royal Society of Chemistry.)

Along the same line, Hu and Yang et al. [49] showed that it was possible to use X-rays to excite LaF_3:Tb scintillating nanoparticles for therapeutic purpose. FRET process was detected in this work.

More recently, Cai et al. [50] reviewed the work of using scintillating nanoparticles for photodynamic therapy. The authors summarized recent publications in this research area, and many rare earth nanoparticles were discussed in their review.

6.3.1.13 Quantum Dots

Quantum dots have been used in X-ray scintillation and imaging. The synthesis and applications of quantum dots have been described in the literature, as recently reviewed by Medintz et al. [51]. Quantum dot nanomaterials are now widely available from many companies. Quantum dots to date are mainly used for generating type 3 physical enhancement. Briefly, quantum dots are made by reducing two or more salts in the presence of high affinity ligands toward the elements in the quantum dots. In a typical synthesis, NaHTe and $Cd(ClO_4)_2$ solutions are reduced by mercaptopropionic acid (MPA) in water. If the surfactants are organic, further chemical modification is needed to make quantum dots soluble in water. Ligand exchange reactions can be used to replace the ligands. In one example, Kang et al. [52] developed a CdTe quantum dot of different sizes. The central wavelength of emission shifted as the size of quantum dots change. The authors also embedded the quantum dots in polymers to form composites.

Beaulieu et al. [53] described the results of coating the surface of CdSe quantum dots with ZnS, CdZnS, and CdS to preserve the fluorescence of CdSe quantum dots under X-ray irradiation. The diameter of these quantum dots with multiple protective layers was 6–8 nm. The radioluminescence decayed mildly under 120 keV X-ray irradiation, dropping only 4% over 2 kGy irradiation, which was three times better than that of uncoated CdSe quantum dots; the latter decreased by 12% after the same dose of irradiation, which was already much better than the behavior of CdSe or CdSe/ZnS quantum dots shown in reports in the literature that showed a 50% drop in radioluminescence after only 100 Gy irradiation. For example, Stodilka et al. [54] reported the behavior of CdSe quantum dots coated with ZnS. Radioluminescence decreased to 20% after irradiation of 100 Gy of 1–2 MV γ-rays. In a similar work, Withers et al. [90] revealed the poor luminescence stability of CdSe/ZnS quantum dots under 662 keV γ-rays. Radioluminescence dropped to 1/e after 200 Gy irradiation.

6.3.1.14 Silicon and Germanium Semiconductor Nanoparticles

Silicon nanoparticles were made in top-down methods by Gonzalez et al. [55] and were used in X-ray nanochemistry by Gonzalez and Kotler et al. [56]. The method of synthesis was electrochemical etching, which was different from the more

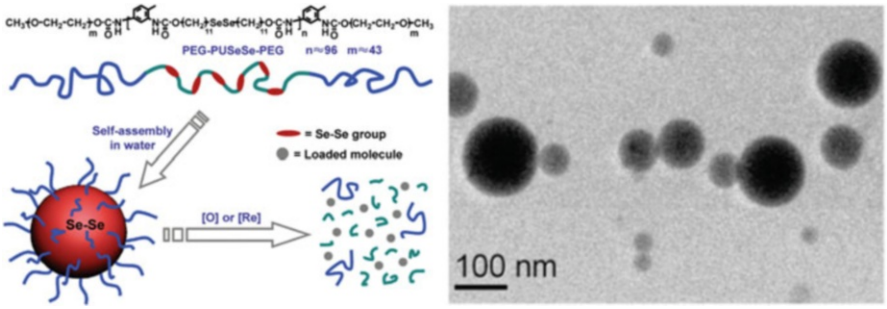

Fig. 6.14 Spherical polymer nanoparticles made of diselenide complexes for X-ray triggered release of payloads. (Adapted with permission from Xu and Zhang et al. [58]. Copyright (2010) American Chemical Society.)

conventional, bottom-up methods developed by Kauzlarich et al. [57]. Electrochemical etching was simpler, though the size control was less precise than the bottom-up method. After sonication to obtain silicon nanoparticles, their surface was functionalized with several ligands including amine and enoate. The size distribution was broad, covering the range of 1–8 nm.

6.3.1.15 Other Spherical Nanoparticles

Several selenium nanomaterials have been made and used to enhance the effectiveness of X-ray irradiation. For example, selenium-selenium polymer nanoparticles were prepared by Xu and Zhang et al. [58]. The nanomaterial was used in several experiments to measure the radiation triggered release of payloads. Figure 6.14 shows the protocol to make the nanoparticles as well as a TEM image of the nanomaterial. In addition, other selenium nanoparticles were used for X-ray enhancement, and the results are shown in Sect. 9.8.

6.3.1.16 Clusters

In addition to nanoparticles, various clusters have been synthesized to improve the efficacy of conversion of X-rays to other forms of energy. For example, Kirakci and Lang et al. [59] synthesized octahedral molybdenum clusters to function as X-ray nanoscintillators. The compound can increase the production of singlet oxygen by absorbing X-rays and emitting 690 nm photons, therefore making it possible to generate X-ray-induced luminescence and singlet oxygen. These properties remained the same when the compound or cluster was embedded in polystyrene films, which further increased the yield of singlet oxygen generation and luminescence through energy transfer from polystyrene to the cluster. Figure 6.15 shows the structure (left panel) of the cluster and an application scheme (right panel).

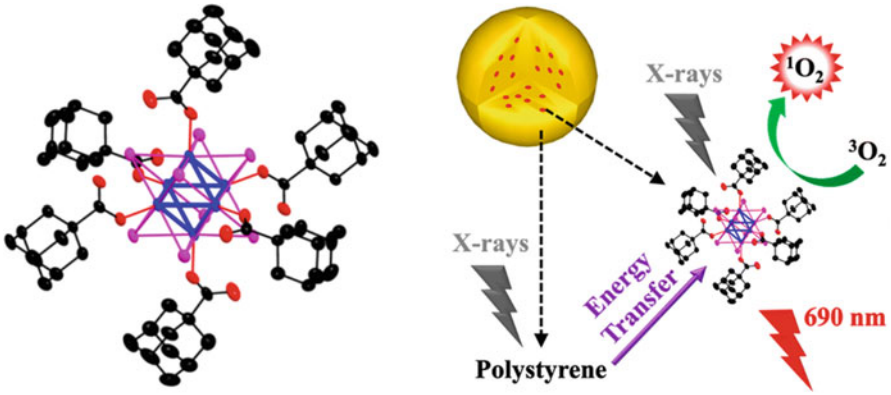

Fig. 6.15 Inorganic clusters made of molybdenum (left panel). The right panel shows how X-rays are used to excite the clusters to produce singlet oxygen. The clusters under X-ray irradiation emit 690 nm light. (Adapted with permission from Kirakci and Lang et al. [59]). Copyright (2016) American Chemical Society.)

6.3.2 Nonspherical Nanoparticles

Besides spherical nanoparticles, other forms of nanomaterials can also enable enhancement to the effectiveness of X-ray irradiation. These nanomaterials are nanotubes, nanorods, nanowires, nanoprisms, and nanodisks. This book does not enumerate all the currently available nanomaterials and only covers those nanomaterials that have been used in X-ray enhancement measurements reported in the literature or those that have been used in the syntheses of nanomaterials for enhancement measurements. For example, Tian and Pan et al. [60] studied PEGylated Au@Pt nanodendrites for CT imaging and radiotherapy. The synthesis began with the synthesis of 8 nm gold nanoparticles. Pt was then incorporated onto the gold nanoparticles by adding $Pt(acac)_2$ and oleylamine. PEG ligands were then conjugated to the surface. The overall diameter of the nanomaterial was 30 nm. The nanomaterial was mildly toxic to cells, with cell viability dropping to 85% at 0.1 mg/mL incubation concentrations.

The most massive nanomaterials used in X-ray enhancement measurements were gold nanowires or nanotubes. They were 100–200 nm in diameter and microns long. These nanotubes packed in solution or space like haystacks and had space voids between the nanotubes for analytes or targets. This nanomaterial created the highest weight percentage (WP) of gold in water, which could potentially produce the highest physical enhancement. However, as it is shown in Chaps. 2 and 5, this was not the case as the surface of bare gold nanomaterials scavenged radicals and reduced the amount of reaction oxygen species.

The synthesis of gold nanotubes employed silica nanowire cores. First, silica nanowires were grown from catalytic reactions using cobalt or other nanoparticles as catalysts based on a method developed by Guo et al. [61]. Two nanometer cobalt

Fig. 6.16 Gold nanotubes made from silica nanowires. The figure shows the silica nanowire (SiNW) core and the gold nanotube coating. (Reprinted from Guo et al. [62]. Copyright (2006), with permission from Elsevier.)

nanoparticle catalysts were deposited on the surface of silicon wafers, which were then placed in a high-temperature furnace. Silane gas was flown through the high-temperature region, and silica nanowires (SiNW) were produced. The wires were collected using a razor blade to peel the silica nanowire film off the wafer. The nanowires were dispersed in water, into which small THPC-covered gold nanoparticle seeds were added and silica nanowires were covered with THPC-covered gold nanoparticles. An aged gold salt aqueous solution and weak reducing agents were added into the gold nanoparticle-coated silica nanowire solution, and gold nanotubes were formed. The synthesis was done at room temperature or in a high-temperature microwave oven autoclave device. The nanotubes grown in the microwave device had a smoother surface. Figure 6.16 shows a typical gold nanotube, exposing a section of SiNW.

The synthesized nanotubes can be directly used for enhancement measurement. However, because microwave synthesis was a surfactant ligand-free method, gold was exposed to the solution and could directly react with reactive oxygen species, which resulted in the destruction of hydroxyl radicals because gold has a lower reduction potential than the hydroxyl radical. Future work will be needed to modify the surface of gold nanotubes so that it does not scavenge reactive oxygen species.

Krishnan et al. [63] synthesized gold nanotriangles and used them in in vitro and in vivo work. Seeded growth methods developed by Murphy et al. [64] were adapted in the nanoprisms or nanotriangle synthesis which used seed gold nanoparticles and cetyltrimethylammonium chloride (CTAC) ligands in multiple growth steps. The nanotriangles were nearly equilateral triangles with an edge length of 61 nm. In vivo results showed mild enhancement; biodistribution results showed a clear accumulation of 5 ppm of the nanomaterials in the tumor. Based on the magnitude of physical enhancement caused by gold nanomaterials shown in Chap. 2, it is clear that the amount of enhancement observed in the work cannot be caused by physical enhancement by the nanomaterials even for only a mild enhancement.

6.3.3 *Aggregated Nanoparticles*

Aggregation of nanomaterials is not preferred in many applications of nanotechnology and nanoscience. Nonetheless, dimers and aggregates can enhance X-ray effects similar to a shell of gold shown in Chap. 2. There are several reports of how to make nanoparticle dimers. The actual syntheses, however, were rather difficult, so more work needs to be done to make nanoparticle dimer synthesis more readily available. Here, several methods are briefly discussed. Nann et al. [65] showed that 10 nm gold nanoparticles were attached to 100 nm silica nanoparticles. Lithography was another approach to make these structures. El-Sayed et al. [66] demonstrated that dimer distance between gold nanoparticles influenced SPR response. It should be pointed out that these aggregates were not used in X-ray nanochemistry measurements.

Tsourkas et al. [67] used oil-water emulsions to trap 1.9 nm gold nanoparticles in small micelles of nanometer sizes. The micelle emulsion was stabilized with amphiphilic diblock copolymer polyethylene oxide (4 k Dalton)-polycaprolactone (3 k Dalton). Both 1.9 nm gold nanoparticles and the polymers were dissolved in toluene, which was then mixed with water. The mixture was emulsified in an ultrasonic bath. Centrifuge separation was used to extract the desired size fraction; small particles were removed via filtration. The final product is shown in Fig. 6.17.

Su et al. [68] used aggregates of gold nanoparticles to fabricate microdisks. A polydimethylsiloxane stamp with the footprint of microdisks was immersed in a polyelectrolyte solution to form a layer of several electrolytes, to which a layer of gold nanoparticles was attached. The diameter of the disks was approximately 5 μm. The height of each electrolyte/gold assembly was approximately 22 nm. Multiple layers of gold and electrolytes were formed. Up to five layers were made in a single disk in the example shown in the report. These disks were then mixed with cells to form cell/disk heterodimers for X-ray enhancement measurements. Figure 6.18 illustrates how the microdisks are made.

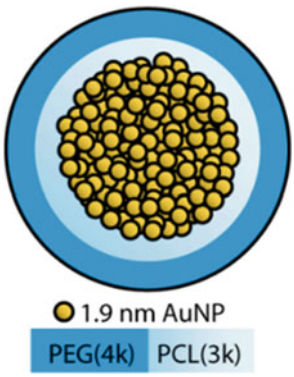

Fig. 6.17 Formation of aggregated gold nanoparticles in micelles. 1.9 nm gold nanoparticles were trapped in micelles. (Adapted with permission from Tsourkas et al. [67]. Copyright (2014) American Chemical Society.)

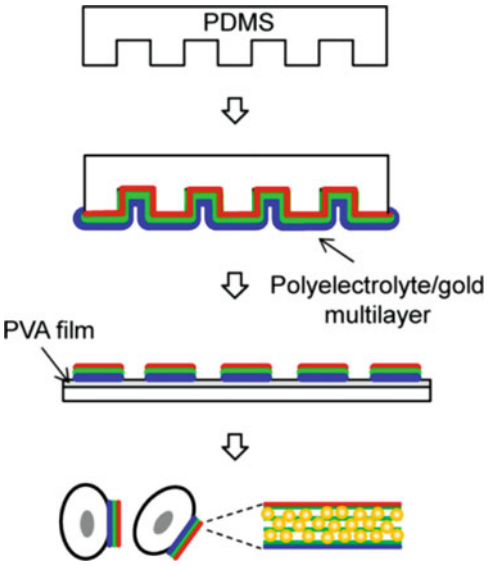

Fig. 6.18 Multilayered gold nanoparticle micro disks for enhancement of the effectiveness of X-ray irradiation. (Adapted with permission from Su et al. [68]. Copyright (2015) American Chemical Society.)

6.3.4 Complex Nanomaterials

These nanomaterials are more than just aggregates of one kind of nanoparticle—the final nanomaterials are assembled from several different kinds of nanomaterials or chemicals. Currently, there are several examples, and much more work can be done in this area. One example showing a glimpse of the potential of these nanomaterials was given by Fologea et al. [69], who assembled several molecular components into a nanoassembly. Figure 9.43 shows the targeted assembly. The authors envisioned a unique application for this nanoassembly. Another complex spherical nanomaterial was synthesized by Xie et al. [70], who assembled a few components to form a nanostructure the authors called SAO that promotes the formation of singlet oxygen while under X-ray irradiation. The nanostructure is shown in Fig. 6.19, which describes a structure of SAO and how it helps production of singlet oxygen.

Bu and Shi et al. [71] synthesized a complex nanomaterial that had a rare earth core and a silica shell covered with photodynamic therapy reagents such as porphyrin IX and targeting ligands such as TAT peptide (GRKKRRQRRRPQ). Porphyrin IX molecules were embedded in silica, and the nanoparticles were also covered with PEG ligands. The overall size of the nanomaterial was approximately 50 nm. The authors named the nanomaterial UCSPs-PEG/TAT, which was responsive to both X-ray and near-infrared irradiation to produce reactive oxygen species. Bu and Shi et al. [72] also reported the synthesis and application of a similar nanomaterial, PEG-USMSs-SNO, that had nitric oxide (NO) donors within the nanoparticles.

Another example was given by Guo et al. [36] who synthesized calcium phosphate-coated liposomes (CaPELs) with aqueous solutions of sulforhodamine B (SRB) trapped inside. SRB was incubated with lipids, and liposomes were formed

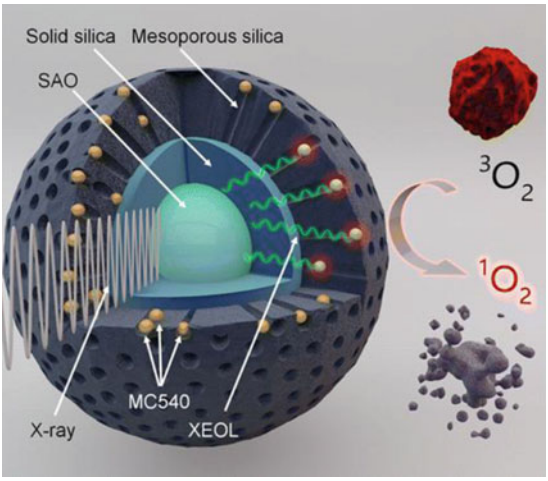

Fig. 6.19 The construction of SAO in silica nanoparticles for conversion of oxygen to singlet oxygen. (Adapted with permission from Xie et al. [70]. Copyright (2015) American Chemical Society.)

through micro-extrusion. Then, phosphoric acid and calcium chloride were used to deposit a calcium phosphate shell on the liposome surface at pH 10. The nanomaterials are shown in Fig. 6.9 and the synthetic method is given in Sect. 6.3.1.6. This nanomaterial can be used to detect type 2 physical enhancement because their size is approximately 100 nm in outer diameter and the solid calcium phosphate shell does not allow radicals to permeate. Other sizes of liposomes and CaPELs can be made, depending on the extrusion process.

Liu et al. [73] developed a new nanomaterial called BM@NCP(DSP)-PEG that had a bovine serum albumin protein-stabilized MnO_2 nanoparticle core wrapped by a polymer-linked cisplatin compound c,c,t-(diamminedichlorodisuccinato)Pt(IV) or DSP shell. Hafnium ions were also incorporated in the shell. This nanomaterial was then coated with dopamine followed by PEG. The overall size of the nanomaterial was slightly less than 110 nm. The Pt compounds were the prodrug.

Tung and Liu et al. [74] synthesized a new nanomaterial with which the authors studied the damage of *E. coli* under X-ray irradiation. The nanoparticle core was made of graphene oxide quantum dots (GQD), which were 3 nm in diameter. The quantum dots were then conjugated to multiple vancomycin molecules, which helped target bacteria, followed by attaching protoporphyrin to the surface of the quantum dots. The final product was a complex nanoparticle consisting of multiple quantum dots, and overall size was approximately 100 nm, based on TEM measurements.

6.4 Surfactants and Conjugation Reactions

Successful synthesis of nanoparticles relies on proper construction of the surface of these nanoparticles. Except for a small number of cases where the surface has the same composition as the core, most nanoparticles have different surface

compositions from the core. Further, the surface of nanoparticles is often modified post-synthesis to increase the functionalities of nanoparticles. These post-synthetic modifications have been developed and will be further explored in the future.

In this section, surfactants of the nanomaterials mentioned in this book and the chemical reactions used to generate these surfaces are described. Although many books have been published on the subject, this section mainly focuses on the discussion of nanomaterials used in X-ray enhancement measurements. Currently, many chemical reactions are used to link or conjugate surfactants to the surface of nanomaterials, and much more future work will undoubtedly expand types of surfactants and chemical means to conjugate surfactants to the surface of nanomaterials.

In the following, ligands or surfactants are listed in the context of X-ray enhancement measurements, followed by discussion of reactions with which one can conjugate surfactants to the surface of nanomaterials for X-ray enhancement measurements. A general discussion on the stability of surfactants is given in Sect. 6.4.3.

6.4.1 Surfactants of Nanomaterials

Surfactants of nanomaterials used in X-ray enhancement measurements have to simultaneously satisfy several requirements. First, surfactants have to make nanomaterials soluble in the media of interest, such as water, blood serum, or alcohol. Secondly, for X-ray enhancement, surfactants have to be non-scavenging toward reactive oxygen species or low-energy electrons if the goal is to cause physical enhancement. Lastly, surfactants may need to have affinity toward targets or probes used in X-ray enhancement.

Table 6.2 shows some of the ligands used as surfactants of nanomaterials employed in X-ray enhancement measurements described in this book. The methods

Table 6.2 List of surfactants of several nanomaterials used in X-ray enhancement measurements

Nanomaterials	Surfactants	MW (amu)
Gold nanoparticles	Citrate acid	50
	Polyethylene glycol (PEG)	2000–5000
	Trimethylammonium (TMA)	200
	Mercaptopropionic acid (MPA)	150
	DNA	Various
	Ethidium bromide	314
Silver nanoparticles	Citrate acid	50
Platinum nanoparticles	Polyvinylpyrrolidone (PVP)	10,000–50,000
Oxide nanoparticles	Silica (Si-OH or Si-O-Si)	18
Rare earth nanoparticles		
Micelles		
Liposomes	Phosphate groups	95
Calcium phosphate-enclosed liposomes	Ca^{2+} or PO_4^{3-}	40

of attaching these surfactants to the surface of nanomaterials will be discussed in Sect. 6.4.2. The molecules range from simple citrate anions to complex polyvinylpyrrolidone (PVP) and even DNA molecules. Almost all of these surfactants are molecular.

6.4.2 *Conjugation Reactions to Attach Surfactants to the Surface of Nanomaterials*

Conjugation of ligands to the surface of nanoparticles can be divided into at least three general categories. Category I conjugation includes processes of attaching surfactants to the surface of nanoparticles during the synthesis of nanoparticles. Nanoparticle synthesis is terminated when all the feedstock of atoms or monomer units are used. Category II conjugation is the replacement of the originally attached surfactants with other surfactants. Category III conjugation includes reactions that link different surfactants to what are already on the surface of nanoparticles. Figure 6.20 illustrates these three conjugation processes. All three categories of reactions are discussed in this section. The order of discussion follows the order of nanomaterials discussed in the last section. The content is limited to nanomaterials used in X-ray enhancement studies.

Since reactions defined in the first category are the most frequently occurring reactions and the other two categories of reactions are usually derived from these reaction products, it is critical to examine category I conjugation reactions. These reactions can be represented by three types. The first type of reaction relates to electrostatic attraction between gold atoms and ionic groups, such as citrate anions. The second type of reaction relates to the formation of covalent bonds such as gold-thiol bonds between thiol-terminated ligands and gold surface atoms. The third type relates to interactions of long ligands or surfactants such as PVP that physically wrap around gold nanoparticles. Figure 6.21 illustrates these three reactions between

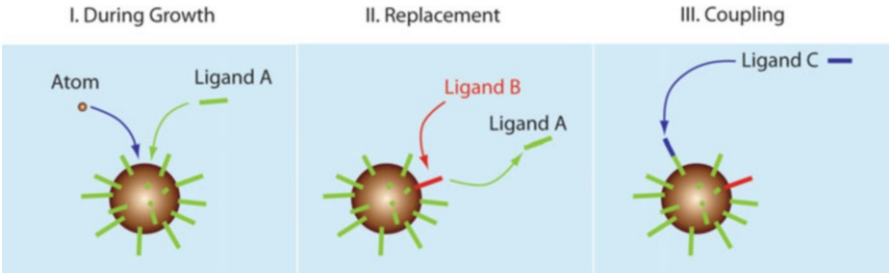

Fig. 6.20 Summary of three categories of chemical reactions linking surfactants to the surface of gold nanoparticles. The first category is addition of surfactant or ligands during or after the growth of nanoparticles. The second category is the replacement of existing surfactants or ligands with other surfactants or ligands. The third connects surfactant ligands of different kinds to the existing surfactants or ligands on the surface

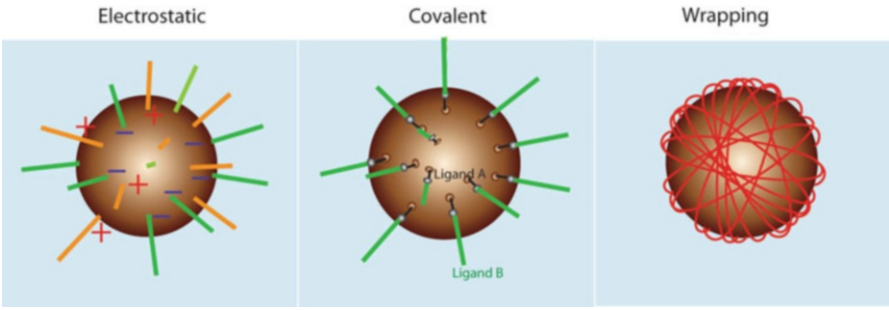

Fig. 6.21 Summary of three types of category I chemical reactions linking surfactants to the surface of gold nanoparticles. The first is addition of ligands during or after the growth of nanoparticles through electrostatic interactions. The second is the conjugation of new ligands to the existing ligands through covalent bonds. The third is addition of long polymeric ligands physically covering the surface

ligands or surfactants and the surface of the nanoparticle. The ligands conjugated to the surface using category I conjugation reactions can then be replaced using category II conjugation reactions or be linked to other ligands through category III conjugation reactions shown in Fig. 6.20.

In the following, published results are discussed based on the categories of reactions through which the surface of nanoparticles are covered. Gold nanoparticles are the most popular nanoparticles used in X-ray enhancement measurements. Synthesis of gold nanoparticles typically involves first or second or both categories of conjugation reactions defined in this section. For instance, only category I conjugation reactions are involved for citrate-covered gold nanoparticles. The average size of gold nanoparticles made this way ranges from 15 to 30 nm. Guo et al. [13] made 15 and 30 nm nanoparticles using citrate reduction and surfactant coverage methods. For smaller and larger gold nanoparticles, more complex synthetic methods were needed. Brust et al. [2] developed the thiol ligand coverage approach that transferred gold nanoparticles from aqueous to organic solvent once gold nanoparticles were covered with thiol ligands. Their method employed category I conjugation reactions. Another example is adding ligands other than the original coverage. For instance, folic acid can be added to the solution of citrate-covered gold nanoparticles. Due to its overwhelmingly high concentration, folic acid ligands are attached to the surface of gold nanoparticles. This approach belongs to category II since folic acid replaces citrate ligands.

To make gold nanoparticles more soluble, stable, or possessing targeting functions, categories II and III conjugation reactions are needed. For example, citrate-covered gold nanoparticles can be made in the first step. In a subsequent step, thiolated polyethylene glycol (PEG) ligands can be used to replace the citrate ligands. PEGylated gold nanoparticles are more soluble in water and more stable in blood serum, making these nanoparticles more suitable for animal studies that demand long circulation times. Guo et al. [13] used these PEGylated gold nanoparticles for type 1 physical and chemical enhancement measurements. Post-

synthesis modification of the surfactants is possible and is often needed in many applications. For example, Guo et al. [1] and Carter et al. [75] showed the switch of ligands to either positive or negative functional groups such as trimethylammonium or carboxylate. Similar methods have been developed by others, such as Rotello et al. [76]. Thiol-glucose ligands were used by several groups including Roa and Xing et al. [77] to improve uptake of gold nanoparticles by cells. DNA ligands can be attached to the surface of gold nanoparticles, a category of reactions that have been extensively studied by Mirkin et al. [78]. In another work in the framework of X-ray enhancement measurements, Su et al. [79] showed the results of ligand replacement reactions involving polyethylenimine (PEI), polysodium sulfonate, polydiallyl-dimethyl ammonium chloride (PDDA), and polydimethylsiloxane ligands.

Most of the third category conjugation reactions involve various click reactions between a ligand already on the surface of the nanoparticles and another incoming ligand. For gold nanoparticles used in X-ray enhancement measurements, click reactions were used by Guo et al. [17] to conjugate doxorubicin (DOX) to DNA bases through succinimidyl 4-(N-maleimidomethly)cyclohexane-1-carboxylate (SMCC). The synthesis conjugated hundreds of 12-mer DNA molecules onto a 15 nm gold nanoparticle, with approximately nine DOX molecules attached to each DNA molecule, resulting in thousands of DOX molecules attached to each gold nanoparticle. In this case, PEGylated gold nanoparticles were used because the nanoparticles were soluble in water during the synthesis. Many similar reactions belonging to thiol-ene click reactions have been extensively studied. Hoyle et al. [80] reviewed the thiol-ene reactions. Dondoni [81] also discussed this process. In another example, Latimer [82], in his MS thesis, discussed the attachment of PEG-CCP ligands onto gold nanoparticles. The modification was extensive, and the work showed the versatility of post-modification. With basic units such as thiol, amine, or carboxylate on the gold surface, other coupling reactions are possible. Castner et al. [83] discussed conjugation between DNA and the gold surface through thiol-ene click reaction. The surface was packed with maleimide ligands for DNA conjugation.

Cheng et al. [84] reported a gold-DOX nanoconjugate. Their method linked DOX to gold through disulfide bonds, which were formed between disulfide terminated PEG ligands on gold nanoparticles Au-PEG-SS and thiolated DOX DOX-SH. The PEG ligands were connected to the gold nanoparticles through thiol-gold bonding. The authors reported the release of DOX when the nanoconjugates were in cells, although it was unclear whether the release was caused by the cleavage of dithiol bonds as the authors claimed or through the cleavage of gold-thiol bond.

Vo-Dinh et al. [85] discussed a method of conjugating ligands to the surface of Y_2O_3 nanoparticles. The first step was to allow decomposed 2-chloroethylphosphonic acid to react with the oxide surface. This reaction belonged to the second category of conjugation reactions shown in Fig. 6.20. This chemical reaction established covalent bonding between the ligand and surface. In the second step, TAT ligands reacted with phosphate functional groups already on the surface of

the oxide nanoparticles. This step belonged to the third category of conjugation reactions shown in Fig. 6.20. As a result, oxide nanoparticles with Psoralen ligands on their surface were prepared. The reaction is shown in Fig. 2.42.

Micelles and liposomes have also been used to construct nanoparticles for X-ray enhancement. Micelles were used to construct gold nanoparticle aggregates. Liposomes were coated with calcium phosphate to prevent permeation of small molecules, such as reactive oxygen species, and the final products were used to study type 2 physical enhancement and X-ray-induced energy transfer (XIET) as studied by Guo et al. [36].

6.4.3 Stability of Ligands on Nanoparticles

As the ligands on the surface (i.e., surfactants) of nanoparticles at least share the control the functionality of nanomaterials, their stability is critical to the success of nanomaterial synthesis and applications. For example, single thiol-gold bonds may be easy to form, but they can also break at room temperature, as demonstrated in many reports. A possible solution is to use multiple thiol-gold bonds to anchor a ligand. For example, Mirkin et al. [86] demonstrated a method to synthesize multiple thiol-anchored DNA conjugates. They observed an approximate five degrees Celsius increase in DNA melting measurements when trithiols were used.

6.5 Characterization of Nanomaterials

Many physical methods can be used to characterize nanomaterials. Some of the most popular methods are listed in Table 6.3. In addition, detection ranges and purposes are given in Table 6.3 as well. Only acronyms of the methods are given. Special methods are being developed. For example, Rotello et al. [87] used mass spectrometry to detect ligands on nanoparticles that may prove useful in future research of nanomaterial synthesis and detection.

6.6 Nanomaterials for Physical, Chemical, and Biological Enhancement

Sections 6.3 and 6.4 describe the nanomaterials and their surfactants used in X-ray nanochemistry. A proper demonstration of each category and type of enhancement described in Chaps. 2, 3, 4, and 5 requires careful choice of these nanomaterials. Here, a number of nanomaterials that satisfy the basic requirements for supporting a particular enhancement are selected. It is important to point out that these

Table 6.3 Detection methods, range and detection purposes of the methods used to characterize nanomaterials

Method	Size range (nm)	Detection	Purposes
TEM	0.1–1000	Positions of atoms	Size, shape, and composition
SEM	1–1000	Positions of atoms	Size, shape, and composition
DLS	1–1000	Mobility of nanoparticles in solutions	Hydrodynamic radius
Mass spectrometry	1–10	Mass of particles or surfactants	Reaction yields or mass of particles
NMR	Any	Nuclear spin	Composition of particles or surfactants
EPR	Any	Unpaired electrons	Composition of particles or surfactants
FTIR	Any	Vibrational modes	Composition of particles, surfactants
UV-Vis	Any	Absorption peaks (valence electrons)	Resonance absorption, absorption profiles/finger print
XAS (EXAFS and XANES)	Any	Absorption spectra (core level)	Average coordination number, disorder, absorption edge, absorption finger prints

requirements are necessary but not sufficient conditions. Other nanomaterials that may not satisfy these conditions can still support these enhancements.

6.6.1 Physical Enhancement

There are at least three types of physical enhancement. Each type requires specific kinds of nanomaterials. General needs for the nanomaterials are discussed here. Although similar discussions are given in Chap. 2, the discussion below is given from the perspective of the nanomaterials that support a specific enhancement type.

6.6.1.1 Type 1 Physical Enhancement

Many nanomaterials can support just type 1 physical enhancement. As stated in Chap. 2, there are several requirements. A brief discussion is provided here relating to the nanomaterials that provide exclusive type 1 physical enhancement.

Silica-Covered 100 nm Gold Nanoparticles

Silica-covered large (>100 nm) gold nanoparticles are one of those that can generate exclusive type 1 physical enhancement, especially when the thickness of the silica

layer is great enough to suppress type 2 physical enhancement but not thick enough to significantly reduce type 1 physical enhancement. For <15 nm thick silica, the attenuation of energetic electrons emitted from the gold nanoparticle core irradiated by 40 keV X-ray energy is only a few percent.

Large Nanoparticles

Large gold nanoparticles (>100 nm) with inert surfactants are another choice. There is no need for silica coating if non-scavenging or weakly scavenging ligands are coated on the surface of these large nanoparticles to make them soluble in water or other media of interest. The reason that large nanoparticles can be used to support type 1 physical enhancement is that their total surface area per unit mass or WP is small; even if their surface is scavenging or catalytically active, as long as the probes are uniformly distributed in the whole sample volume, then it is still possible to generate high and dominating type 1 physical enhancement using large amounts of these nanomaterials. However, the ligand-covered gold surface is still scavenging, resulting in reduction to the enhancement. Non-fluorescent oxide nanoparticles that do not support type 3 physical enhancement can also support type 1 physical enhancement. However, in this case, type 2 physical enhancement still contributes to the measured enhancement, although it is only a small fraction of type 1 physical enhancement.

6.6.1.2 Type 2 Physical Enhancement

Type 2 physical enhancement can be generated by any size gold nanoparticles or nanostructures. As shown in Chap. 2, type 2 physical enhancement dominates in the surface region. The larger the nanomaterial or nanostructure, the greater the magnitude of peak type 2 physical enhancement is. For spherical nanoparticles, type 2 physical enhancement is strongest directly at the surface of the nanoparticle and quickly diminishes as the point of interest moves away from the surface.

Type 2 physical enhancement is more difficult to probe and therefore requires more elaborately designed nanomaterials. To date, the only nanomaterial that supports type 2 physical enhancement measurements was calcium phosphate-enclosed liposomes (CaPELs) with an aqueous solution of sulforhodamine B (SRB) molecules trapped inside, developed by Guo et al. [36]. The size of liposomes was approximately 60 nm in this experimental demonstration. Upon mixing with gold nanoparticles, CaPELs formed transient heterodimers with gold nanoparticles. The concentration of gold nanoparticles was high enough to generate a very strong type 2 physical enhancement signal. The CaP shell casing was thick and solid enough to prevent permeation of reactive oxygen species, but thin enough so that low-energy electrons could still penetrate through it to deposit energy inside CaPELs.

The synthetic approach to make type 2 physical enhancement probes employed by Guo et al. [36] can be expanded. For example, it is possible to use various sizes of

"inner tubes" such as micelles to replace liposomes so that smaller nanoscale probes may be synthesized. It is also possible to have multiple gold nanoparticles attached to a single nanoscale probe to generate much a higher type 2 physical enhancement. However, in this case, the size of gold nanoparticles will have to be smaller, and, consequently, the magnitude of type 2 physical enhancement is smaller, making it more difficult to observe type 2 physical enhancement. Future synthetic work is needed to improve linking multiple large gold nanoparticles to a single CaPEL.

Other attempts have been made to measure type 2 physical enhancement. One example was given by Guo et al. [75] in which gold nanoparticles were attached to supercoiled DNA. However, in that example, the small gold nanoparticles were catalytically active and therefore could be scavenging hydroxyl radicals or enhancing DNA stand breaks through catalytic reactions. Future work is needed to fully understand the results, starting with designing the nanomaterials that support only type 2 physical enhancement.

6.6.1.3 Type 3 Physical Enhancement

Type 3 physical enhancement is more complex than type 1 physical enhancement in the sense that nanomaterials that produce type 3 physical enhancement need to not only absorb X-rays but also need to convert the absorbed energy to UV-Vis photons, a process generally accomplished through the use of semiconductor or rare earth nanoparticles, as well as fluorescent molecules, as discussed in Sects. 2.4.4 and 6.3.1.11.

A number of nanomaterials can meet these requirements. For example, rare earth nanomaterials, quantum dots, and fluorescent semiconductor nanomaterials, such as tungsten oxide nanoparticles, can all meet these requirements. A list of nanomaterials was given in the review by Cai et al. [50]. Future work in the area of combining molecular fluorophores to X-ray absorbing and X-ray scintillating nanomaterials will help create much better type 3 physical enhancement nanomaterials. Nanomaterials that do not strongly absorb X-rays can also support type 3 physical enhancement when they can interact with Compton electrons produced in water under X-ray irradiation to generate UV-Vis photons.

6.6.2 Chemical Enhancement

Chemical enhancement requires completely different types of nanomaterials than type 1 or 2 physical enhancement, especially type 1 physical enhancement. This is because chemical enhancement derives from reactions involving the surface of nanomaterials and X-ray-generated species in media or other species. Therefore, it requires large surface areas as well as catalytically active surfaces. Type 2 physical enhancement does not require the use of an actual surface; it just needs to be close to the surface. Chemical enhancement may still occur even if the surface is covered

with ligands or surfactants, as long as these surfactants are permeable to the reactive oxygen species.

It is possible that certain nanoparticles can simultaneously satisfy the requirements for physical and chemical enhancement. Another option is to mix different nanoparticles that support different categories of enhancement to achieve a higher total enhancement. Guo et al. [88] showed algorithms governing how total enhancements were dependent on the individual enhancements, a topic covered in Chap. 5.

Semiconductor nanomaterials absorb X-rays to generate electron-hole pairs. If the pairs, in the form of exciton, can migrate to the surface of nanomaterials to enable catalytic reactions to produce reactive oxygen species, the nanomaterial can also cause chemical enhancement. Photocatalysis described in Chap. 11 belongs to this process. However, X-ray photocatalysis has not been extensively studied.

6.6.2.1 Anti-Enhancement

Although unintended, physical and chemical enhancement generally shun away from anti-enhancement. However, if no specific actions are taken during synthesis and purification process of nanomaterials, then nanomaterials are often radical scavengers because the surface material or the surfactants can scavenge reactive oxygen species responsible for enhancement. In many cases, anti-enhancement may dominate or even annihilate enhancement generated by nanomaterials. Figure 6.22 shows a few pathways through which nanomaterials can scavenge reactive oxygen species. Pathway A shows direct scavenging of ROS by the surface. Pathway B represents scavenging of ROS by a terminal group on the ligand. Pathway C

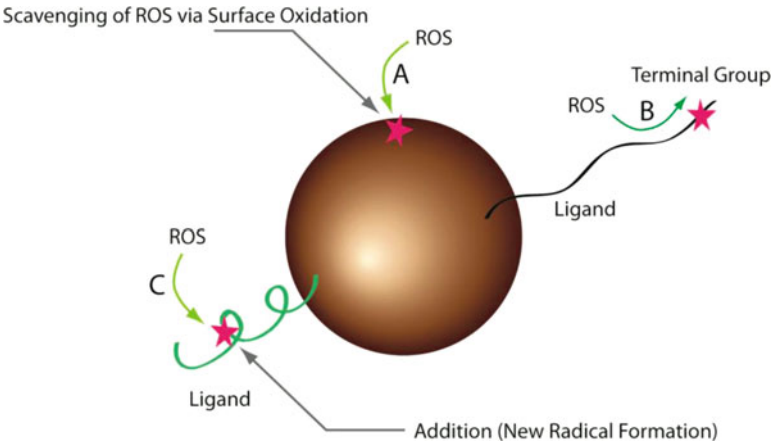

Fig. 6.22 Three different ways for a nanoparticle to scavenge reactive oxygen species (ROS). All three pathways lead to anti-enhancement. Pathway A is scavenging of ROS by the surface. Pathway B is the reaction of ROS with terminal functional groups of the ligand. Pathway C is the formation of a new radical after ROS react with the surfactant

illustrates ROS reacting with the ligand. If anti-enhancement is to be maximized, then these pathways can be utilized. On the other hand, many practices can help reduce anti-enhancement. Choice of surfactants, post-synthesis purification, selection of X-ray energy, choice of nanoparticle size, and the use of scavengers can all be used to control the degree of scavenging by nanomaterials.

6.6.3 Nanomaterials for Other Enhancements

Although biological enhancement is still a largely unknown process, many different types of nanomaterials can enable biological enhancement based on the existing understandings. According to the results presented in Chap. 4, biological enhancement exists when small nanoparticles or unprotected nanoparticles are used because these nanomaterials can bind to biomolecules and interfere with their functions, such as DNA repair, or cause oxidative stress. When large nanoparticles are used, they may not enter the nuclei of cells. For bacteria cells, chemical enhancement may exist for even large gold nanoparticles, and the enhancement may be amplified by cells to result in biological enhancement. In the case of bacteria, the requirement for the size is relaxed. There may be other requirements for nanoparticles to support biological enhancement, which will be studied in the future.

6.7 Nanoparticles for Applications in X-Ray Nanochemistry

Being able to create enhancement of the effectiveness of X-ray irradiation is the basic demand for nanomaterials used in X-ray nanochemistry. Enhancements discussed in Chaps. 2, 3, 4, and 5 have enabled many applications that are discussed in Chaps. 8, 9, 10, and 11. Mukherjee et al. [89] stated that gold nanoparticles were biologically viable and highly adaptable for conjugation with nearly any compound having an amine or thiol functional groups. It is to be seen whether other nanomaterials can surpass gold nanomaterials to dominate the application field of X-ray nanochemistry. In many of those applications, which are dominated by applications in medicine so far, there are additional requirements on the nanomaterials beyond the need for enhancement. These requirements, such as targeting tumors, are briefly discussed in Chap. 9. Requirements for nanomaterials used in imaging are different, which are discussed in Chap. 9 as well.

6.8 Conclusions and Future Work

One of the most important aspects of X-ray nanochemistry is the development of nanomaterials, which helps advance both basic and applied aspects of X-ray nanochemistry. Relevant nanomaterials and various ways to synthesize these nanomaterials are cursorily discussed here. The synthetic requirements for ideal nanomaterials used in X-ray nanochemistry are often more stringent than what are presented here because of the greater need for isolation, optimization, and combination of enhancements offered by these optimized nanomaterials. Currently there are many categories and types of enhancement, and there are nanomaterials that support each of them. This does not mean the nanomaterials are optimized for these enhancements—it simply means the nanomaterials developed to date can at least minimally support these basic enhancement categories and types.

Future efforts should be directed to the improvement of existing nanomaterials so that each category or type of enhancement can be isolated, optimized, and then recombined. These efforts will help improve understanding of the enhancement as well. For instance, better nanoscale probes will help detect type 2 physical enhancement when placed near nanostructures. Even more promising are the nanomaterials that can generate chemical enhancement by improving and incorporating new catalysis and catalysts. For example, more synergistic and catalytically active nanomaterials may enable much stronger chemical enhancement. The biggest breakthroughs in X-ray nanochemistry could happen in this area in the near future. Furthermore, advanced enhancement mechanisms may require nanomaterials to possess even more demanding and distinguished properties. In addition, all these studies can greatly benefit from more advanced theoretical approaches because currently no theoretical basis has been established to satisfactorily explain chemical and biological enhancement observed in X-ray nanochemistry. From these perspectives, X-ray nanochemistry will see a much more rigorous and exciting period of development in the next decade.

References

1. Foley, E., Carter, J., Shan, F., & Guo, T. (2005). Enhanced relaxation of nanoparticle-bound supercoiled DNA in X-ray radiation. *Chemical Communications*, 3192–3194.
2. Brust, M., Walker, M., Bethell, D., Schiffrin, D. J., & Whyman, R. (1994). Synthesis of thiol-Derivatised gold nanoparticles in a 2-phase liquid-liquid system. *Journal of the Chemical Society, Chemical Communications, 0*, 801–802.
3. Hainfeld, J. F., Slatkin, D. N., & Smilowitz, H. M. (2004). The use of gold nanoparticles to enhance radiotherapy in mice. *Physics in Medicine and Biology, 49*, N309–N315.
4. Chithrani, B. D., Ghazani, A. A., & Chan, W. C. W. (2006). Determining the size and shape dependence of gold nanoparticle uptake into mammalian cells. *Nano Letters, 6*, 662–668.
5. Hainfeld, J. F., Smilowitz, H. M., O'Connor, M. J., Dilmanian, F. A., & Slatkin, D. N. (2013). Gold nanoparticle imaging and radiotherapy of brain tumors in mice. *Nanomedicine, 8*, 1601–1609.

6. Ozin, G. A., & Arsenault, A. C. (2005). *Nanochemistry: A chemical approach to nanomaterials*. Cambridge, UK: RSC Publishing.
7. Dreaden, E. C., Alkilany, A. M., Huang, X. H., Murphy, C. J., & El-Sayed, M. A. (2012). The golden age: Gold nanoparticles for biomedicine. *Chemical Society Reviews, 41*, 2740–2779.
8. Brust, M., & Kiely, C. J. (2002). Some recent advances in nanostructure preparation from gold and silver particles: A short topical review. *Colloid and Surface A, 202*, 175–186.
9. Kim, B., Han, G., Toley, B. J., Kim, C. K., Rotello, V. M., & Forbes, N. S. (2010). Tuning payload delivery in tumour cylindroids using gold nanoparticles. *Nature Nanotechnology, 5*, 465–472.
10. Zhang, X. D., Luo, Z. T., Chen, J., Song, S. S., Yuan, X., Shen, X., Wang, H., Sun, Y. M., Gao, K., Zhang, L. F., et al. (2015). Ultrasmall glutathione-protected gold nanoclusters as next generation radiotherapy sensitizers with high tumor uptake and high renal clearance. *Scientific Reports UK, 5*, 8669.
11. Tien, J., Terfort, A., & Whitesides, G. M. (1997). Microfabrication through electrostatic self-assembly. *Langmuir, 13*, 5349–5355.
12. McIntosh, C. M., Esposito, E. A., Boal, A. K., Simard, J. M., Martin, C. T., & Rotello, V. M. (2001). Inhibition of DNA transcription using cationic mixed monolayer protected gold clusters. *Journal of the American Chemical Society, 123*, 7626–7629.
13. Cheng, N. N., Starkewolf, Z., Davidson, A. R., Sharmah, A., Lee, C., Lien, J., & Guo, T. (1950). Chemical enhancement by nanomaterials under X-ray irradiation. *Journal of the Chemical Society, Communications, 2012*(134), 1950–1953.
14. Duff, D., Baiker, A., Gameson, I., & Edwards, P. (1993). A new hydrosol of gold clusters .2. A comparison of some different measurement techniques. *Langmuir, 9*, 2310–2317.
15. Duff, D. G., Baiker, A., & Edwards, P. P. (1993). A new hydrosol of gold clusters .1. Formation and particle-size variation. *Langmuir, 9*, 2301–2309.
16. Turkevich, J., Stevenson, P. C., & Hillier, J. (1951). A study of the nucleation and growth processes in the synthesis of colloidal gold. *Discussions of the Faraday Society, 11*, 55–75.
17. Starkewolf, Z. B., Miyachi, L., Wong, J., & Guo, T. (2013). X-ray triggered release of doxorubicin from nanoparticle drug carriers for cancer therapy. *Chemical Communications, 49*, 2545–2547.
18. Perrault, S. D., & Chan, W. C. W. (2009). Synthesis and surface modification of highly monodispersed, spherical gold nanoparticles of 50-200 nm. *Journal of the American Chemical Society, 131*, 17042–17043.
19. Davidson, R. A., & Guo, T. (2014). Average physical enhancement by nanomaterials under X-ray irradiation. *Journal of Physical Chemistry C, 118*, 30221–30228.
20. Wang, C. H., Hua, T. E., Chien, C. C., Yu, Y. L., Yang, T. Y., Liu, C. J., Leng, W. H., Hwu, Y., Yang, Y. C., Kim, C. C., et al. (2007). Aqueous gold nanosols stabilized by electrostatic protection generated by X-ray irradiation assisted radical reduction. *Materials Chemistry and Physics, 106*, 323–329.
21. Liu, C. J., Wang, C. H., Chien, C. C., Yang, T. Y., Chen, S. T., Leng, W. H., Lee, C. F., Lee, K. H., Hwu, Y., Lee, Y. C., et al. (2008). Enhanced x-ray irradiation-induced cancer cell damage by gold nanoparticles treated by a new synthesis method of polyethylene glycol modification. *Nanotechnology, 19*, 1–5. Article ID 295104.
22. Liu, C. J., Wang, C. H., Chen, S. T., Chen, H. H., Leng, W. H., Chien, C. C., Wang, C. L., Kempson, I. M., Hwu, Y., Lai, T. C., et al. (2010). Enhancement of cell radiation sensitivity by pegylated gold nanoparticles. *Physics in Medicine and Biology, 55*, 931–945.
23. Kumar, R., Korideck, H., Ngwa, W., Berbeco, R. I., Makrigiorgos, G. M., & Sridhar, S. (2013). Third generation gold nanoplatform optimized for radiation therapy. *Translational Cancer Research, 2*, 228.
24. Wang, C. H., Chien, C. C., Yu, Y. L., Liu, C. J., Lee, C. F., Chen, C. H., Hwu, Y., Yang, C. S., Je, J. H., & Margaritondo, G. (2007). Structural properties of 'naked' gold nanoparticles formed by synchrotron X-ray irradiation. *Journal of Synchrotron Radiation, 14*, 477–482.

25. Merga, G., Saucedo, N., Cass, L. C., Puthussery, J., & Meisel, D. (2010). "Naked" gold nanoparticles: Synthesis, characterization, catalytic hydrogen evolution, and SERS. *Journal of Physical Chemistry C, 114*, 14811–14818.
26. Evanoff, D. D., & Chumanov, G. (2005). Synthesis and optical properties of silver nanoparticles and arrays. *Chemphyschem, 6*, 1221–1231.
27. Ziegler, C., & Eychmuller, A. (2011). Seeded growth synthesis of uniform gold nanoparticles with diameters of 15-300 nm. *Journal of Physical Chemistry C, 115*, 4502–4506.
28. Bastús, N. G., Comenge, J., & Puntes, V. (2011). Kinetically controlled seeded growth synthesis of citrate-stabilized gold nanoparticles of up to 200 nm: Size focusing versus Ostwald ripening. *Langmuir, 27*, 11098–11105.
29. Liu, X. K., Xu, H. L., Xia, H. B., & Wang, D. Y. (2012). Rapid seeded growth of monodisperse, quasi-spherical, citrate-stabilized gold nanoparticles via H_2O_2 reduction. *Langmuir, 28*, 13720–13726.
30. Song, H., Rioux, R. M., Hoefelmeyer, J. D., Komor, R., Niesz, K., Grass, M., Yang, P. D., & Somorjai, G. A. (2006). Hydrothermal growth of mesoporous SBA-15 silica in the presence of PVP-stabilized Pt nanoparticles: Synthesis, characterization, and catalytic properties. *Journal of the American Chemical Society, 128*, 3027–3037.
31. Porter, R., Shan, F., & Guo, T. (2005). Coherent anti-stokes Raman scattering microscopy with spectrally tailored ultrafast pulses. *The Review of Scientific Instruments, 76*, 043108.
32. Jin, R. C., Jureller, J. E., Kim, H. Y., & Scherer, N. F. (2005). Correlating second harmonic optical responses of single Ag nanoparticles with morphology. *Journal of the American Chemical Society, 127*, 12482–12483.
33. Solomon, S. D., Bahadory, M., Jeyarajasingam, A. V., Rutkowsky, S. A., Boritz, C., & Mulfinger, L. (2007). Synthesis and study of silver nanoparticles. *Journal of Chemical Education, 84*, 322–325.
34. Yu, X. J., Li, A., Zhao, C. Z., Yang, K., Chen, X. Y., & Li, W. W. (2017). Ultrasmall semimetal nanoparticles of bismuth for dual-modal computed tomography/photoacoustic imaging and synergistic thermoradiotherapy. *ACS Nano, 11*, 3990–4001.
35. Davidson, R. A., & Guo, T. (2012). An example of X-ray nanochemistry: SERS investigation of polymerization enhanced by nanostructures under X-ray irradiation. *Journal of Physical Chemistry Letters, 3*, 3271–3275.
36. Sharmah, A., Yao, Z., Lu, L., & Guo, T. (2016). X-ray-induced energy transfer between nanomaterials under X-ray irradiation. *Journal of Physical Chemistry C, 120*, 3054–3060.
37. Schulzendorf, M., Cavelius, C., Born, P., Murray, E., & Kraus, T. (2011). Biphasic synthesis of $Au@SiO_2$ core-shell particles with stepwise ligand exchange. *Langmuir, 27*, 727–732.
38. Shankar, C., Dao, A. T. N., Singh, P., Higashimine, K., Mott, D. M., & Maenosono, S. (2012). Chemical stabilization of gold coated by silver core-shell nanoparticles via electron transfer. *Nanotechnology, 23*, 245704.
39. Lien, J., Peck, K. A., Su, M. Q., & Guo, T. (2016). Sub-monolayer silver loss from large gold nanospheres detected by surface plasmon resonance in the sigmoidal region. *Journal of Colloid and Interface Science, 479*, 173–181.
40. Huang, C. W., Kearney, V., Moeendarbari, S., Jiang, R. Q., Christensen, P., Tekade, R., Sun, X. K., Mao, W. H., & Hao, Y. W. (2015). Hollow gold nanoparticles as biocompatible Radiosensitizer: An in vitro proof of concept study. *Journal of Nano Research Sw, 32*, 106–U140.
41. Huang, C. W., Jiang, J. C., Lu, M. Y., Sun, L., Meletis, E. I., & Hao, Y. W. (2009). Capturing electrochemically evolved Nanobubbles by electroless deposition. A facile route to the synthesis of hollow nanoparticles. *Nano Letters, 9*, 4297–4301.
42. Moeendarbari, S., Tekade, R., Mulgaonkar, A., Christensen, P., Ramezani, S., Hassan, G., Jiang, R., Oz, O. K., Hao, Y. W., & Sun, X. K. (2016). Theranostic Nanoseeds for efficacious internal radiation therapy of unresectable solid tumors. *Scientific Reports UK, 6*, 20614.

43. Milosavljevic, B. H., Pimblott, S. M., & Meisel, D. (2004). Yields and migration distances of reducing equivalents in the radiolysis of silica nanoparticles. *The Journal of Physical Chemistry. B, 108*, 6996–7001.
44. Nakayama, M., Sasaki, R., Ogino, C., Tanaka, T., Morita, K., Umetsu, M., Ohara, S., Tan, Z. Q., Nishimura, Y., Akasaka, H., et al. (2016). Titanium peroxide nanoparticles enhanced cytotoxic effects of X-ray irradiation against pancreatic cancer model through reactive oxygen species generation in vitro and in vivo. *Radiation Oncology, 11*, 91.
45. Chen, Y. Y., Song, G. S., Dong, Z. L., Yi, X., Chao, Y., Liang, C., Yang, K., Cheng, L., & Liu, Z. (2017). Drug-loaded mesoporous tantalum oxide nanoparticles for enhanced synergetic chemoradiotherapy with reduced systemic toxicity. *Small, 13*, 1602869.
46. Xing, M. M., Cao, W. H., Pang, T., Ling, X. Q., & Chen, N. (2009). Preparation and characterization of monodisperse spherical particles of X-ray nano-phosphors based on Gd_2O_2S:Tb. *Chinese Science Bulletin, 54*, 2982–2986.
47. Townley, H. E., Kim, J., & Dobson, P. J. (2012). In vivo demonstration of enhanced radiotherapy using rare earth doped titania nanoparticles. *Nanoscale, 4*, 5043–5050.
48. Elmenoufy, A. H., Tang, Y. A., Hu, J., Xu, H. B., & Yang, X. L. (2015). A novel deep photodynamic therapy modality combined with CT imaging established via X-ray stimulated silica-modified lanthanide scintillating nanoparticles. *Chemical Communications, 51*, 12247–12250.
49. Tang, Y. G., Hu, J., Elmenoufy, A. H., & Yang, X. L. (2015). Highly efficient FRET system capable of deep photodynamic therapy established on X-ray excited mesoporous LaF3:Tb scintillating nanoparticles. *ACS Applied Materials & Interfaces, 7*, 12261–12269.
50. Kamkaew, A., Chen, F., Zhan, Y. H., Majewski, R. L., & Cai, W. B. (2016). Scintillating nanoparticles as energy mediators for enhanced photodynamic therapy. *ACS Nano, 10*, 3918–3935.
51. Algar, W. R., Prasuhn, D. E., Stewart, M. H., Jennings, T. L., Blanco-Canosa, J. B., Dawson, P. E., & Medintz, I. L. (2011). The controlled display of biomolecules on nanoparticles: A challenge suited to bioorthogonal chemistry. *Bioconjugate Chemistry, 22*, 825–858.
52. Kang, Z. T., Zhang, Y. L., Menkara, H., Wagner, B. K., Summers, C. J., Lawrence, W., & Nagarkar, V. (2011). CdTe quantum dots and polymer nanocomposites for x-ray scintillation and imaging. *Applied Physics Letters, 98*, *181914*.
53. Delage, M. E., Lecavalier, M. E., Cloutier, E., Lariviere, D., Allen, C. N., & Beaulieu, L. (2016). Robust shell passivation of CdSe colloidal quantum dots to stabilize radioluminescence emission. *AIP Advances, 6*, 105011.
54. Stodilka, R. Z., Carson, J. J. L., Yu, K., Zalman, M. B., Li, C. S., & Wilkinson, D. (2009). Optical degradation of CdSe/ZnS quantum dots upon gamma-ray irradiation. *Journal of Physical Chemistry C, 113*, 2580–2585.
55. Romero, J. J., Llansola-Portoles, M. J., Dell'Arciprete, M. L., Rodriguez, H. B., Moore, A. L., & Gonzalez, M. C. (2013). Photo luminescent 1-2 nm sized silicon nanoparticles: A surface-dependent system. *Chemistry of Materials, 25*, 3488–3498.
56. Gara, P. M. D., Garabano, N. I., Portoles, M. J. L., Moreno, M. S., Dodat, D., Casas, O. R., Gonzalez, M. C., & Kotler, M. L. (2012). ROS enhancement by silicon nanoparticles in X-ray irradiated aqueous suspensions and in glioma C6 cells. *Journal of Nanoparticle Research, 14*, 741.
57. Baldwin, R. K., Pettigrew, K. A., Ratai, E., Augustine, M. P., & Kauzlarich, S. M. (2002). Solution reduction synthesis of surface stabilized silicon nanoparticles. *Chemical Communications*, 1822–1823.
58. Ma, N., Li, Y., Xu, H. P., Wang, Z. Q., & Zhang, X. (2010). Dual redox responsive assemblies formed from diselenide block copolymers. *Journal of the American Chemical Society, 132*, 442.
59. Kirakci, K., Kubat, P., Fejfarova, K., Martincik, J., Nikl, M., & Lang, K. (2016). X-ray inducible luminescence and singlet oxygen sensitization by an octahedral molybdenum cluster compound: A new class of nanoscintillators. *Inorganic Chemistry, 55*, 803–809.

60. Liu, X., Zhang, X., Zhu, M., Lin, G. H., Liu, J., Zhou, Z. F., Tian, X., & Pan, Y. (2017). PEGylated Au@Pt nanodendrites as novel theranostic agents for computed tomography imaging and photothermal/radiation synergistic therapy. *ACS Applied Materials & Interfaces, 9*, 279–285.
61. Qu, Y. Q., Carter, J. D., & Guo, T. (2006). Silica nanocoils. *The Journal of Physical Chemistry. B, 110*, 8296–8301.
62. Qu, Y. Q., Carter, J. D., Sutherland, A., & Guo, T. (2006). Surface modification of gold nanotubules via microwave radiation, sonication and chemical etching. *Chemical Physics Letters, 432*, 195–199.
63. Bhattarai, S. R., Derry, P. J., Aziz, K., Singh, P. K., Khoo, A. M., Chadha, A. S., Liopo, A., Zubarev, E. R., & Krishnan, S. (2017). Gold nanotriangles: Scale up and X-ray radiosensitization effects in mice. *Nanoscale, 9*, 5085–5093.
64. Gole, A., & Murphy, C. J. (2004). Seed-mediated synthesis of gold nanorods: Role of the size and nature of the seed. *Chemistry of Materials, 16*, 3633–3640.
65. Dewi, M. R., Gschneidtner, T. A., Elmas, S., Ranford, M., Moth-Poulsen, K., & Nann, T. (2015). Monofunctionalization and dimerization of nanoparticles using coordination chemistry. *ACS Nano, 9*, 1434–1439.
66. Jain, P. K., & El-Sayed, M. A. (2007). Universal scaling of plasmon coupling in metal nanostructures: Extension from particle pairs to nanoshells. *Nano Letters, 7*, 2854–2858.
67. Al Zaki, A., Joh, D., Cheng, Z. L., De Barros, A. L. B., Kao, G., Dorsey, J., & Tsourkas, A. (2014). Gold-loaded polymeric micelles for computed tomography-guided radiation therapy treatment and radiosensitization. *ACS Nano, 8*, 104–112.
68. Zhang, P. P., Qiao, Y., Xia, J. F., Guan, J. J., Ma, L. Y., & Su, M. (2015). Enhanced radiation therapy with multilayer microdisks containing Radiosensitizing gold nanoparticles. *ACS Applied Materials & Interfaces, 7*, 4518–4524.
69. Fologea, E., Salamo, G., Henry, R., Borrelli, M. J., & Corry, P. M. (2010). Method of controlling drug release from a liposome carrier. US Patent: US8808733B2.
70. Chen, H. M., Wang, G. D., Chuang, Y. J., Zhen, Z. P., Chen, X. Y., Biddinger, P., Hao, Z. L., Liu, F., Shen, B. Z., Pan, Z. W., et al. (2015). Nanoscintillator-mediated X-ray inducible photodynamic therapy for in vivo cancer treatment. *Nano Letters, 15*, 2249–2256.
71. Fan, W. P., Shen, B., Bu, W. B., Zheng, X. P., He, Q. J., Cui, Z. W., Ni, D. L., Zhao, K. L., Zhang, S. J., & Shi, J. L. (2015). Intranuclear biophotonics by smart design of nuclear-targeting photo−/radio-sensitizers co-loaded upconversion nanoparticles. *Biomaterials, 69*, 89–98.
72. Fan, W. P., Wenbo, B., Bu, Z. Z., Shen, B., Zhang, H., He, Q. J., Ni, D. L., Cui, Z. W., Zhao, K. L., Bu, J. W., et al. (2015). X-ray radiation-controlled NO-release for on-demand depth-independent hypoxic radiosensitization. *Angewandte Chemie International Edition, 54*, 14026–14030.
73. Liu, J. J., Chen, Q., Zhu, W. W., Yi, X., Yang, Y., Dong, Z. L., & Liu, Z. (2017). Nanoscale-coordination-polymer-shelled manganese dioxide composite nanoparticles: A multistage redox/pH/H2O2-responsive cancer theranostic nanoplatform. *Advanced Functional Materials, 27*, 1605926.
74. Pan, C. L., Chen, M. H., Tung, F. I., & Liu, T. Y. (2017). A nanovehicle developed for treating deep-seated bacteria using low-dose X-ray. *Acta Biomaterialia, 47*, 159–169.
75. Carter, J. D., Cheng, N. N., Qu, Y. Q., Suarez, G. D., & Guo, T. (2007). Nanoscale energy deposition by x-ray absorbing nanostructures. *The Journal of Physical Chemistry. B, 111*, 11622–11625.
76. Rotello, V. M., Ghosh, P., Han, G., De, M., & Kim, C. K. (2008). Gold nanoparticles in delivery applications. *Advanced Drug Delivery Reviews, 60*, 1307–1315.
77. Zhang, X. J., Xing, J. Z., Chen, J., Ko, L., Amanie, J., Gulavita, S., Pervez, N., Yee, D., Moore, R., & Roa, W. (2008). Enhanced radiation sensitivity in prostate cancer by gold-nanoparticles. *Clinical and Investigative Medicine, 31*, E160–E167.

78. Demers, L. M., Ginger, D. S., Park, S. J., Li, Z., Chung, S. W., & Mirkin, C. A. (2002). Direct patterning of modified oligonucleotides on metals and insulators by dip-pen nanolithography. *Science, 296*, 1836–1838.
79. Zhang, P. P., Qiao, Y., Wang, C. M., Ma, L. Y., & Su, M. (2014). Enhanced radiation therapy with internalized polyelectrolyte modified nanoparticles. *Nanoscale, 6*, 10095–10099.
80. Hoyle, C. E., & Bowman, C. N. (2010). Thiol-Ene click chemistry. *Angewandte Chemie International Edition, 49*, 1540–1573.
81. Dondoni, A. (2008). The emergence of thiol-Ene coupling as a click process for materials and bioorganic chemistry. *Angewandte Chemie International Edition, 47*, 8995–8997.
82. Latimer, C. L. (2013). *Octaarginine labelled 30 nm gold nanoparticles as agents for enhanced radiotherapy*. In Department of Medical Biophysics, University of Toronto, Toronto, Vol. Master of science, p 81.
83. Lee, C. Y., Gong, P., Harbers, G. M., Grainger, D. W., Castner, D. G., & Gamble, L. J. (2006). Surface coverage and structure of mixed DNA/alkylthiol monolayers on gold: Characterization by XPS, NEXAFS, and fluorescence intensity measurements. *Analytical Chemistry, 78*, 3316–3325.
84. Gu, Y. J., Cheng, J. P., Man, C. W. Y., Wong, W. T., & Cheng, S. H. (2012). Gold-doxorubicin nanoconjugates for overcoming multidrug resistance. *Nanomedicine Nanotechnology, 8*, 204–211.
85. Scaffidi, J. P., Gregas, M. K., Lauly, B., Zhang, Y., & Vo-Dinh, T. (2011). Activity of psoralen-functionalized nanoscintillators against cancer cells upon X-ray excitation. *ACS Nano, 5*, 4679–4687.
86. Li, Z., Jin, R. C., Mirkin, C. A., & Letsinger, R. L. (2002). Multiple thiol-anchor capped DNA-gold nanoparticle conjugates. *Nucleic Acids Research, 30*, 1558–1562.
87. Zhu, Z. J., Tang, R., Yeh, Y. C., Miranda, O. R., Rotello, V. M., & Vachet, R. W. (2012). Determination of the intracellular stability of gold nanoparticle monolayers using mass spectrometry. *Analytical Chemistry, 84*, 4321–4326.
88. Davidson, R. A., & Guo, T. (2015). Multiplication algorithm for combined physical and chemical enhancement of X-ray effect by nanomaterials. *Journal of Physical Chemistry C, 119*, 19513–19519.
89. Kudgus, R. A., Szabolcs, A., Khan, J. A., Walden, C. A., Reid, J. M., Robertson, J. D., Bhattacharya, R., & Mukherjee, P. (2013). Inhibiting the growth of pancreatic adenocarcinoma in vitro and in vivo through targeted treatment with designer gold nanotherapeutics. *PLoS One, 8*, e57522.
90. Withers, N J., Plumley, J. B., Triño, N. D., Sankar, K., Akins, B. A., Rivera, A. C., Smolyakov, G. A., Timmins, G. S., & Osiński, M. (2009). Scintillating-nanoparticle-induced enhancement of absorbed radiation dose. *Proc. of SPIE, 7189*, 718917